

# Hierarchy of many-body invariants and quantized magnetization in anomalous Floquet insulators

Frederik Nathan<sup>1</sup>, Dmitry A. Abanin<sup>2</sup>, Netanel H. Lindner<sup>3</sup>, Erez Berg<sup>4,5</sup>, and Mark S. Rudner<sup>1</sup>

<sup>1</sup>*Center for Quantum Devices, Niels Bohr Institute,  
University of Copenhagen, 2100 Copenhagen, Denmark*

<sup>2</sup>*Department of Theoretical Physics, University of Geneva, 1211 Geneva, Switzerland*

<sup>3</sup>*Physics Department, Technion, 320003 Haifa, Israel*

<sup>4</sup>*Department of Physics, University of Chicago, Chicago, IL 60637, USA*

<sup>5</sup>*Department of Condensed Matter Physics, The Weizmann Institute of Science, Rehovot, 76100, Israel*  
(Dated: July 30, 2019)

The anomalous Floquet insulator (AFI) is an intrinsically nonequilibrium topological phase that arises in disordered, periodically driven systems. In the noninteracting case, the nontrivial topology of the AFI gives rise to a quantized current at the edge, and a quantized magnetization in the bulk. Recent work indicates that the AFI is compatible with many-body localization, and is thus stable in the presence of interactions. Here we study the bulk topological properties of the AFI in the interacting case. Compared with the non-interacting case, interactions lead to an enrichment of the topological phase diagram: we find that the AFI is characterized by a family of bulk topological invariants, which are encoded in the time-averaged magnetization density operator of the system. A nontrivial value of the  $\ell$ -th invariant signifies a quantized contribution to the magnetization density in filled regions arising from correlated  $\ell$ -particle circulating orbits. The non-interacting “anomalous Floquet-Anderson insulator” (AFAI) is characterized by a nonzero value of the first invariant, with all higher invariants equal to zero. We discuss novel strongly correlated anomalous phases, with nonzero values of higher invariants, that are topologically distinct from the AFAI.

In recent years, periodic driving has been extensively studied as a means for realizing nontrivial topological phases of matter<sup>1–18</sup>. An important result of this work has been the discovery of a wide range of new intrinsically non-equilibrium topological phases of matter, which have no equilibrium counterparts<sup>8,9,16–34</sup>. These “anomalous” phases are characterized by robust properties of their micromotion (i.e., the dynamics that takes place within a driving period), such as frequency-locked oscillations in Floquet time crystals<sup>24–27</sup>, or quantized orbital magnetization density in the two-dimensional anomalous Floquet-Anderson insulator (AFAI)<sup>9,29,30</sup>.

Disorder plays a crucial role for stabilizing Floquet phases in closed systems. In the presence of interactions, disorder-induced many-body localization (MBL) provides a mechanism for the system to avoid uncontrollably absorbing energy from the driving field, and thereby to retain nontrivial properties at long times<sup>35–37</sup>. Importantly, the requirement of many-body localization does not preclude the system from exhibiting a variety of types of symmetry-breaking and topological order<sup>24,25,38</sup>.

In this paper we characterize the topological properties of time-evolution in many-body localized two-dimensional periodically driven systems of fermions<sup>35–38</sup> (see Fig. 1). Our work is motivated by recent results which strongly suggest that this class of systems can support a nontrivial topological phase, known as the Anomalous Floquet Insulator<sup>38</sup> (AFI), which can be seen as the generalization of the AFAI to interacting systems (see Refs. 29 and 30). Despite being localized and insulating, the AFI features nontrivial circulating currents in the bulk, which in the noninteracting case (the AFAI) give rise to quantized orbital magnetization<sup>29</sup>. In a ge-

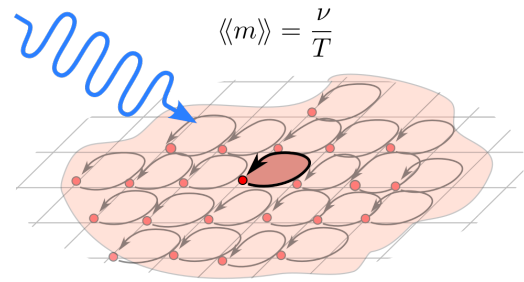


FIG. 1. Schematic depiction of the two-dimensional anomalous Floquet insulator. This interacting phase is characterized by driving-induced circular motion of bulk particles, and is described by a family of integer-valued topological invariants  $\{\mu_\ell\}$  that are protected by localization. Nontrivial topology reveals itself in a quantized, nonzero magnetization density within regions where all states are filled, given by  $\langle m \rangle = \frac{1}{T} \sum_\ell \mu_\ell$ .

ometry with boundaries, the AFI supports thermalizing chiral edge states coexisting with a localized bulk<sup>30,38</sup>. Focusing on the bulk, by analyzing the evolution and magnetization density operators of the system in a geometry without edges, in this work we uncover a family of new topological phases which are distinguished by the nature of the circulating currents that they host.

The phases that we identify are characterized by a family of integer-valued bulk topological invariants,  $\{\mu_\ell\}$ . These invariants characterize the Fock space evolution operator of the system as a whole, independent of any particular state. Once a specific number of particles is present, and a state specified, the nontrivial topology en-

coded in the invariants  $\{\mu_\ell\}$  is manifested as a quantized magnetization density in any filled region of the lattice, as schematically depicted in Fig. 1. Interestingly, in the absence of interactions, only a single one of these invariants ( $\mu_1$ ) can be nonzero; this invariant is the topologically-quantized orbital magnetization found in Ref. 29. With interactions, higher invariants can become nonzero. Generalizing the orbital magnetization captured by  $\mu_1$ , these higher invariants can be associated with correlated circulating orbits of two or more particles.

When one or more of the higher invariants are nonzero, the system is in a new, strongly-correlated, intrinsically non-equilibrium phase that is qualitatively distinct from the (noninteracting) AFAI. Our results thus reveal the existence of a whole family of new topological phases, some of which are topologically distinct from the AFAI and the AFI introduced above. Broadening the definition, we refer to all such phases characterized by nonzero values of one or more of the invariants  $\{\mu_\ell\}$  as (two-dimensional) *anomalous Floquet insulators* (AFIs). We present an explicit example demonstrating that nonzero values of the higher invariants may be realized in models with correlated hoppings.

Interestingly, the arguments establishing the topological protection of the invariant  $\mu_\ell$  do not rely on full many-body localization in the thermodynamic limit; rather only *partial* localization (i.e., localization of all states consisting of up to  $k$  particles) is necessary. Hence, even for systems that are not strictly MBL in the thermodynamic limit, one or more of the invariants  $\mu_\ell$  can still be defined. Thus it may be possible to see signatures of these new invariants at finite times (i.e., before thermalization occurs) in systems that are not fully MBL.

The rest of the paper is organized as follows. In Sec. I we briefly review the structure of the Floquet operator in many-body localized systems, and of the orbital magnetization operator. From the time-averaged magnetization density operator, we identify a set of topological invariants  $\{\mu_\ell\}$  that characterize the AFI phase (Sec. II). We show that nonzero values of the invariants give rise to a quantized magnetization density in regions where all sites are occupied (Sec. II.E). In Sec. III we discuss the nature of the higher-order invariants which are only present in interacting systems. We support our conclusions with numerical simulations (Sec. IV) and conclude with a discussion (Sec. V).

## I. STRUCTURE OF THE FLOQUET OPERATOR

In the following sections, we characterize the AFI by establishing a topological classification of time-evolution in two-dimensional periodically-driven many-body localized fermionic systems. As a preliminary step, in this section we review the structure of the Floquet operator in many-body localized fermionic systems, and explain how micromotion in such systems is characterized by the

orbital magnetization density.

The system we study is a two-dimensional lattice system of interacting fermions, of physical dimensions  $L \times L$ , subject to periodic driving. While our results apply to any type of lattice, we assume for simplicity that the system is defined on a square lattice with (time-dependent) nearest-neighbor tunneling and lattice constant  $a$ . In later sections we study models with correlated hopping, where similar arguments can be applied. The time evolution of the system is described by the time-periodic Hamiltonian  $H(t) = H(t + T)$ , where  $T$  is the driving period; we assume for now that the system is fully many-body localized due to strong disorder. To avoid complications from the coexistence of thermalizing chiral edge states and a many-body localized bulk<sup>38</sup>, we focus on the case where the system is defined on a torus, such that no edges are present. A detailed study of the interplay between delocalized edge states and MBL in the bulk is left for future work; some aspects have been discussed in Refs. 38 and 39.

Due to MBL, the system has a complete set of emergent local integrals of motion<sup>36,37,40,41</sup> (LIOMs),  $\{\hat{n}_\alpha\}$ . The LIOMs form a mutually commuting set of quasilocal operators that are individually preserved by the stroboscopic evolution of the system. The number of independent LIOMs in the localized system is given by the dimension  $D$  of the system's single-particle Hilbert space. For spinless fermions with one orbital per site, we have  $D = L^2/a^2$ . The LIOMs  $\{\hat{n}_\alpha\}$  may thus be labelled by a single index  $\alpha$  which runs from 1 to  $D$ .

To make the discussion more concrete, the LIOMs can be identified from the system's Floquet operator<sup>36</sup>,  $U(T) \equiv \mathcal{T}e^{-i\int_0^T dt H(t)}$ . (We work in units where  $\hbar = 1$  throughout.) Specifically, the Floquet operator takes the form  $U(T) = e^{-iH_{\text{eff}}T}$ , where

$$H_{\text{eff}} = \sum_{\alpha_1} \varepsilon_{\alpha_1} \hat{n}_{\alpha_1} + \sum_{\alpha_1, \alpha_2} \varepsilon_{\alpha_1 \alpha_2} \hat{n}_{\alpha_1} \hat{n}_{\alpha_2} + \cdots \quad (1)$$

Each coefficient  $\varepsilon_{\alpha_1 \dots \alpha_k}$  (referred to as a quasienergy coefficient in the following) is associated with a particular combination  $\hat{n}_{\alpha_1} \dots \hat{n}_{\alpha_k}$  formed from the  $D$  distinct LIOMs, and has units of energy. Each sum  $\sum_{\alpha_1 \dots \alpha_k}$  in Eq. (1) runs over all  $\binom{D}{k}$  distinct combinations of  $k$  LIOMs, where  $\binom{D}{k}$  denotes the binomial coefficient. The above form of the Floquet operator implies that each LIOM  $\hat{n}_\alpha$  is preserved by the stroboscopic evolution of the system, and thus the operators  $\{\hat{n}_\alpha\}$  are integrals of motion.

In the following, we use the LIOM structure of the Floquet operator and several important properties of the LIOMs, which we now review, to identify the invariants  $\{\mu_\ell\}$  that characterize the AFI phase. Firstly, each LIOM  $\hat{n}_\alpha$  can be written in the form of a fermionic counting operator:  $\hat{n}_\alpha = \hat{f}_\alpha^\dagger \hat{f}_\alpha$ , where  $\hat{f}_\alpha$  is a (dressed) quasilocal fermionic annihilation operator. The fermionic annihilation operator  $\hat{f}_\alpha$  is constructed from the original lattice annihilation and creation operators  $\{\hat{c}_i\}$  and

$\{\hat{c}_i^\dagger\}$ , respectively, as:  $\hat{f}_\alpha = \sum_i \psi_i^\alpha \hat{c}_i + \sum_{ijk} \psi_{ijk}^\alpha \hat{c}_i^\dagger \hat{c}_j \hat{c}_k + \sum_{i\dots m} \psi_{ijklm}^\alpha \hat{c}_i^\dagger \hat{c}_j^\dagger \hat{c}_k \hat{c}_l \hat{c}_m + \dots$ , where  $\hat{c}_i$  annihilates a fermion on site  $i$  in the lattice. Through the identification of the LIOMs with fermionic counting operators, we note that  $\sum_\alpha \hat{n}_\alpha$  gives the total number of fermions in the system.

Another crucial property of the LIOMs is that each LIOM  $\hat{n}_\alpha$  has its support localized around a particular location  $\mathbf{r}_\alpha$  in the lattice. Specifically, the magnitude of the coefficient  $\psi_{i_1\dots i_k}^\alpha$  decreases exponentially with the distance  $s$  from any of the sites  $i_1, \dots, i_k$  to  $\mathbf{r}_\alpha$ :  $\psi_{i_1\dots i_k}^\alpha \sim e^{-s/\xi_f}$ , where the length scale  $\xi_f$  sets the spatial extent of the LIOMs. Similarly to the LIOMs, the quasienergy coefficients  $\{\varepsilon_{\alpha_1\dots\alpha_k}\}$  also exhibit localized behavior. Specifically,  $\varepsilon_{\alpha_1\dots\alpha_k}$  decays as  $e^{-d/\xi_\varepsilon}$ , where  $d$  is the distance between any two of the LIOM centers  $\mathbf{r}_{\alpha_1} \dots \mathbf{r}_{\alpha_k}$ ; here  $\xi_\varepsilon$  is another localization length scale (not necessarily identical to  $\xi_f$ , see Ref. 42).

The LIOM decomposition above defines a labelling for the eigenstates of the Floquet operator (referred to as Floquet eigenstates), which we use extensively below. Specifically, we let  $|\Psi_{\alpha_1\dots\alpha_k}\rangle$  denote the  $k$ -particle Floquet eigenstate that satisfies  $\hat{n}_\alpha |\Psi_{\alpha_1\dots\alpha_k}\rangle = |\Psi_{\alpha_1\dots\alpha_k}\rangle$  if  $\alpha \in \{\alpha_1 \dots \alpha_k\}$ , while  $\hat{n}_\alpha |\Psi_{\alpha_1\dots\alpha_k}\rangle = 0$  if  $\alpha \notin \{\alpha_1 \dots \alpha_k\}$ . Correspondingly,  $E_{\alpha_1\dots\alpha_k}$  denotes the quasienergy of the Floquet eigenstate  $|\Psi_{\alpha_1\dots\alpha_k}\rangle$ . By acting with  $H_{\text{eff}}$  on the state  $|\Psi_{\alpha_1\dots\alpha_k}\rangle$ , we obtain the following relationship between the quasienergy  $E_{\alpha_1\dots\alpha_k}$  and the quasienergy coefficients in Eq. (1):

$$E_{\alpha_1\dots\alpha_k} = \sum_i \varepsilon_{\alpha_i} + \sum_{i,j}' \varepsilon_{\alpha_i\alpha_j} + \dots, \quad (2)$$

where the  $m$ -th sum above runs over all  $\binom{k}{m}$  distinct choices of  $m$  LIOM indices among the  $k$  indices  $\alpha_1 \dots \alpha_k$ .

Note that MBL systems may be characterized by several distinct localization lengths<sup>42</sup>. In particular, the LIOM expansion above establishes two length scales,  $\xi_f$  and  $\xi_\varepsilon$ . In the following, we will make use of an additional relevant length scale,  $\xi_L$ , which characterizes the spread of time-evolved operators.

## II. TOPOLOGICAL INVARIANTS OF THE TIME EVOLUTION

In this section, we characterize the micromotion of many-body localized systems. We show that such systems may exhibit non-trivial micromotion, featuring steady-state circulating currents at long times. We characterize these circulating currents by analyzing the time-averaged magnetization density operator of the system. From this analysis we identify a set of topological invariants  $\{\mu_\ell\}$  that characterize the circulating steady-state currents that the system may support.

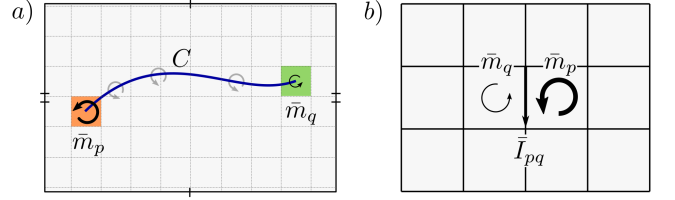


FIG. 2. a) Schematic depiction of the relationship between current and magnetization density [Eq. (5)]. In many-body localized systems, the time-averaged current passing through a cut  $C$  is determined by the difference between the currents circulating around the cut's two end-points,  $p$  and  $q$ . The currents circulating around plaquette  $p$  are measured by the magnetization density operator  $\bar{m}_p$ . b) Ampere's law on the lattice. The difference in magnetization densities between two adjacent plaquettes  $p$  and  $q$  gives the current  $\bar{I}_{pq}$  on the bond between them.

### A. Characterization of micromotion

Naively, one might expect that the time-averaged current density in a many-body localized system always vanishes due to localization. Indeed, in MBL systems, there can be no net flow of charge across any closed curve. However, for an *open* curve (or “cut”), as schematically depicted in Fig. 2a, a nonzero time-averaged current may run across the cut due to uncompensated local circulating currents around the curve's endpoints. The total current circulating around a point in a given plaquette is precisely the magnetization density in this plaquette.

To establish this relationship in more rigorous terms, we consider the total time-averaged current that passes through a cut  $C$  between plaquettes  $p$  and  $q$  in the lattice, as depicted in Fig. 2a. The operator  $I_C(t)$  measuring the current through the cut  $C$  is given by

$$I_C(t) = \sum_{b \in B_C} I_b(t), \quad (3)$$

where  $I_b$  denotes the bond current operator on bond  $b$ , and the sum runs over the set  $B_C$  of all bonds that cross the cut  $C$  [see Appendix A for an explicit definition of  $I_b(t)$ ]. Note that  $I_b(t)$ , and thereby  $I_C(t)$ , depends on time in the Schrödinger picture due to the explicit time-dependence of the Hamiltonian  $H(t)$ .

To characterize the circulating currents in the system, we seek the long-time-averaged expectation value of the current  $\langle\langle I_C \rangle\rangle$  for an arbitrary initial state,  $|\psi\rangle$ . Here we introduce the notation  $\langle\langle \mathcal{O} \rangle\rangle \equiv \lim_{\tau \rightarrow \infty} \frac{1}{\tau} \int_0^\tau dt \langle \psi(t) | \mathcal{O}(t) | \psi(t) \rangle$  to indicate time-averaged expectation values. The time-averaged current  $\langle\langle I_C \rangle\rangle$  may equivalently be computed in the Heisenberg picture as  $\langle\langle I_C \rangle\rangle = \langle \psi | \bar{I}_C | \psi \rangle$ , where  $|\psi\rangle$  denotes the initial state of the system, and  $\bar{I}_C$  denotes the long-time-average of the current operator  $I_C$  in the Heisenberg picture<sup>43</sup>:

$$\bar{I}_C = \lim_{\tau \rightarrow \infty} \frac{1}{\tau} \int_0^\tau dt U^\dagger(t) I_C(t) U(t). \quad (4)$$

For later, we define  $\bar{\mathcal{O}} \equiv \lim_{\tau \rightarrow \infty} \frac{1}{\tau} \int_0^\tau dt U^\dagger(t) \mathcal{O}(t) U(t)$ .

As argued above, the time-averaged current  $\bar{I}_C$  across cut  $C$  can only exhibit a nonzero expectation value due to localized circulating currents at the cut's two endpoints,  $p$  and  $q$ . This in turn implies that  $\bar{I}_C$  should only depend on the details of the system near plaquettes  $p$  and  $q$ . This intuition is verified in Appendix A, where we prove that  $\bar{I}_C$  only has support near the two endpoints of the cut  $C$ . Specifically, assuming only MBL and conservation of charge, we show that  $\bar{I}_C$  must take the form

$$\bar{I}_C = \bar{m}_p - \bar{m}_q, \quad (5)$$

where the operator  $\bar{m}_p$  has its full support (up to an exponentially small correction) within a distance  $\xi_l$  from plaquette  $p$ , and similarly for  $\bar{m}_q$ . Here  $\xi_l$  is a finite length scale measuring the spread of operators in the system: specifically, for any time-periodic operator  $A(t)$  with a finite region of support  $R$ , the long-time average  $\bar{A}$  is a local integral of motion with support within a finite distance  $\xi_l$  from  $R$  (up to an exponentially small correction)<sup>44</sup>.

Crucially, the operator  $\bar{m}_p$  in Eq. (5) is the same for *any* cut with an endpoint in plaquette  $p$ . Thus, Eq. (5) uniquely defines the operator  $\bar{m}_p$  for each plaquette  $p$  in the system, up to a correction exponentially small in system size. Specifically, let plaquette  $q$  be separated from plaquette  $p$  by a distance  $d$ , of order the system size,  $L$ . In this case,  $\bar{m}_p$  can be identified uniquely from the terms of  $\bar{I}_C$  which have support nearest to plaquette  $p$ , up to a correction of order  $\mathcal{O}(e^{-d/\xi_l}) \sim \mathcal{O}(e^{-L/\xi_l})$ .

The operator  $\bar{m}_p$  for each plaquette  $p$  may be defined from Eq. (5) by considering a cut of length  $\sim L$  (up to an exponentially small correction). The set of operators  $\{\bar{m}_p\}$  obtained in this way then obey Eq. (5) for *any* two plaquettes in the lattice. In particular, when the plaquettes  $p$  and  $q$  are adjacent, Eq. (5) implies that  $\bar{m}_p - \bar{m}_q = \bar{I}_{pq}$ , where  $\bar{I}_{pq}$  measures the time-averaged current on the bond separating plaquettes  $p$  and  $q$ , as schematically depicted in Fig. 2b. This relationship is the time-averaged lattice version of Ampere's law, which relates the current density,  $\mathbf{j}$ , to the magnetization density,  $\mathbf{m}$ :  $\mathbf{j} = \nabla \times \mathbf{m}$  (see Ref. 29). We thus identify the operator  $\bar{m}_p$  as the time-averaged magnetization density in the system at plaquette  $p$ <sup>45</sup>. As the above discussion shows, the time-averaged magnetization  $\bar{m}_p$  measures the total current circulating around plaquette  $p$ .

In the following section we show that, remarkably, the trace of the magnetization density operator  $\bar{m}_p$  is *quantized*. The quantized trace of  $\bar{m}_p$  characterizes the topology of the time-evolution and serves as a topological order parameter for the AFI phase.

### 1. Definition of $\bar{m}_p$ from response to magnetic flux

To prove the quantization of the trace of  $\bar{m}_p$ , we express the magnetization density in terms of the system's response to a magnetic field. Specifically, we show that

the difference  $\bar{m}_p - \bar{m}_q$  is given by the time-averaged response of the Hamiltonian to the insertion of a magnetic flux  $\phi_{pq}$  through plaquette  $p$ , while a compensating flux  $-\phi_{pq}$  is inserted through plaquette  $q$  (such that the net flux through the surface of the torus remains constant).

As a first step in making the connection, we note that the insertion of the magnetic flux  $\phi_{pq}$  can be realized by assigning a Peierls' phase  $\theta_b = \phi_{pq}$  to each bond  $b$  that crosses a cut  $C$  between the two plaquettes<sup>46</sup>, as depicted, e.g., in Fig. 2a. Specifically, we assign a phase factor  $e^{-i\phi_{pq}}$  to each term in the Hamiltonian that accounts for tunneling across  $C$  in the direction counter-clockwise with respect to plaquette  $p$ . We assign the conjugate phase factor to terms accounting for tunneling in the opposite direction, thereby ensuring Hermiticity of the Hamiltonian. With this choice of gauge, the Hamiltonian's response to the flux  $\phi_{pq}$  is given by

$$\frac{\partial H(t)}{\partial \phi_{pq}} = \sum_{b \in B_C} \frac{\partial H(t)}{\partial \theta_b}. \quad (6)$$

Here  $\frac{\partial H(t)}{\partial \theta_b}$  denotes the Hamiltonian's response to the application of a Peierls' phase on the bond  $b$ , and  $B_C$  denotes the set of all bonds that cross the cut  $C$ .

As a next step, we note that the Schrödinger picture bond current operator  $I_b(t)$  on bond  $b$  is given by the Hamiltonian's response to a Peierls' phase on this bond:  $I_b(t) = -\frac{\partial H(t)}{\partial \theta_b}$ . Thus, using Eq. (3), we conclude that

$$-\frac{\partial H(t)}{\partial \phi_{pq}} = I_C(t), \quad (7)$$

where  $I_C(t)$  denotes the total current passing through the cut  $C$ .

Finally, we consider the time-average of  $\frac{\partial H(t)}{\partial \phi_{pq}}$  in the Heisenberg picture,  $\overline{\frac{\partial H}{\partial \phi_{pq}}}$  [see definition below Eq. (4)]. Using Eqs. (5) and (7), we find

$$-\overline{\frac{\partial H}{\partial \phi_{pq}}} = \bar{m}_p - \bar{m}_q, \quad (8)$$

where  $\bar{m}_p$  and  $\bar{m}_q$  are the same local operators identified in Eq. (5). Below, we use Eq. (8) to show that  $\text{Tr}(\bar{m}_p)$  is quantized.

Note that the quantization of magnetic flux through the torus prevents us from defining  $\bar{m}_p$  from the response of the Hamiltonian to a flux through a single plaquette  $p$  on the torus. Specifically, since the total flux through the torus must be quantized as an integer multiple of the flux quantum, the magnetic flux  $\phi_p$  through plaquette  $p$  can only be varied continuously if a compensating flux  $-\phi_p$  is inserted elsewhere in the system. Hence the derivative  $\frac{\partial H}{\partial \phi_p}$  with respect to the flux in a *single* plaquette is by itself not well-defined on the torus. However, remarkably, MBL allows us to isolate a local operator corresponding to the magnetization density on plaquette  $p$  through the well-defined operator  $\frac{\partial H(t)}{\partial \phi_{pq}}$  as outlined above.

## B. Topological invariance of $\text{Tr}_k \bar{m}_p$

In the previous section we introduced the time-averaged magnetization density  $\bar{m}_p$ , which characterizes steady-state circulating currents in many-body localized systems. As a main result of this paper, we now show that, for each value of  $k$ , the trace of  $\bar{m}_p$  in the  $k$ -particle subspace is a quantized topological invariant of the system. The topological properties of the AFI phases are fully characterized by the numbers  $\text{Tr}_1 \bar{m}_p, \text{Tr}_2 \bar{m}_p, \text{Tr}_3 \bar{m}_p \dots$ , where  $\text{Tr}_k(\mathcal{O})$  denotes the trace of the operator  $\mathcal{O}$  in the  $k$ -particle subspace.

We prove the topological invariance of  $\text{Tr}_k \bar{m}_p$  through a simple line of arguments. First, Eq. (5) implies:

$$\text{Tr}_k \bar{m}_p - \text{Tr}_k \bar{m}_q = \text{Tr}_k \bar{I}_C. \quad (9)$$

Using the cyclic property of the trace and  $U(t)U^\dagger(t) = \mathbf{1}$ , we have  $\text{Tr}_k \bar{I}_C = \lim_{\tau \rightarrow \infty} \frac{1}{\tau} \int_0^\tau dt \text{Tr}_k I_C(t)$ . Recall from Eq. (3) that the current operator  $I_C(t)$  is given by a sum of bond current operators. Noting that any bond current operator  $I_b(t)$  is by construction traceless (see Appendix A), we conclude that  $\text{Tr}_k \bar{I}_C = 0$ . Hence we find:

$$\text{Tr}_k \bar{m}_p = \text{Tr}_k \bar{m}_q. \quad (10)$$

This relation holds for *any* pair of plaquettes in the lattice. Therefore, for a given disorder realization,  $\text{Tr}_k \bar{m}_p$  must take the same universal value for all plaquettes in the system.

We now show that the universal value of  $\text{Tr}_k \bar{m}_p$  is a topological invariant of the system in the thermodynamic limit ( $L \rightarrow \infty$ )<sup>47</sup>. To show this, consider smoothly changing the parameters of  $H(t)$  in some region  $R$  of the system in such a way that MBL is preserved. We recall that  $\bar{m}_p$  exclusively depends on the details of the system around the plaquette  $p$ , up to an exponentially small correction (due to the exponentially decaying tails of the LIOMs). Hence, for a plaquette  $p_0$  located a distance of order  $L/2$  from the region  $R$ , the trace  $\text{Tr}_k \bar{m}_{p_0}$  may only change by an amount of order  $e^{-L/2\xi_l}$  during the deformation. Note that, due to Eq. (10),  $\text{Tr}_k \bar{m}_p$  must be given by the same value for *all* plaquettes, throughout the deformation. Even when the plaquette  $p$  is located within the region  $R$  where  $H(t)$  is perturbed,  $\text{Tr}_k \bar{m}_p$  can only change by an amount of order  $e^{-L/2\xi_l}$  during the deformation.

The global parameters of the system can be changed by a sequence of local perturbations of the type described above. Thus  $\text{Tr}_k \bar{m}_p$  must remain invariant under any smooth change of the system that preserves MBL, up to a correction exponentially small in  $L$ . In particular, in the thermodynamic limit  $L \rightarrow \infty$ ,  $\text{Tr}_k \bar{m}_p$  remains constant under any smooth, MBL-preserving deformation. Thus,  $\text{Tr}_k \bar{m}_p$  is a topological invariant of the system.

The topological invariant  $\text{Tr}_k \bar{m}_p$  is protected by MBL. Specifically, since  $\bar{m}_p$  is only well-defined for MBL systems (see discussion in the end of Sec. II.A.1), the value of  $\text{Tr}_k \bar{m}_p$  can change if the system goes from one MBL phase to another through a delocalization transition.

## C. “Natural” basis of invariants

The above discussion shows that for each  $k$ , the  $k$ -particle trace of the magnetization density,  $\text{Tr}_k \bar{m}_p$ , is a topological invariant. The topological invariants  $\text{Tr}_1 \bar{m}_p, \text{Tr}_2 \bar{m}_p, \dots$  hence characterize the topology of the time-evolution operator in two-dimensional many-body localized systems. However, as we find below, the invariants  $\text{Tr}_k \bar{m}_p$  depend on the size of the system, and are thus not intrinsic quantities. For instance, in noninteracting systems,  $\text{Tr}_k \bar{m}_p$  scales as  $L^{2(k-1)}$ , where  $L$  is the physical dimension of the system<sup>48</sup>. In this subsection we construct linear combinations of the invariants  $\{\text{Tr}_k \bar{m}_p\}$  that give an equivalent set of (system size independent) invariants  $\{\mu_\ell\}$  that characterize the *intrinsic* topological properties of the system.

The intrinsic invariants  $\{\mu_\ell\}$  are conveniently expressed in terms of the LIOMs that were introduced in Sec. I. Since the long-time average of any Heisenberg picture operator is diagonal in the basis of Floquet eigenstates<sup>49</sup>, the operator  $\bar{m}_p$  must be an integral of motion<sup>50</sup>. This requires  $\bar{m}_p$  to take the following form in terms of the LIOMs  $\{\hat{n}_\alpha\}$  introduced in Eq. (1):

$$\bar{m}_p = \sum_{\alpha_1} m_{\alpha_1}^p \hat{n}_{\alpha_1} + \sum_{\alpha_1 \alpha_2} m_{\alpha_1 \alpha_2}^p \hat{n}_{\alpha_1} \hat{n}_{\alpha_2} + \dots \quad (11)$$

Here, for each term involving a products of  $\ell$  LIOMs, the sum  $\sum_{\alpha_1 \dots \alpha_\ell}$  runs over the  $\binom{D}{\ell}$  distinct combinations of  $\ell$  LIOM indices  $\alpha_1 \dots \alpha_\ell$ . Due to the finite support of the operator  $\bar{m}_p$ , we note that the coefficient  $m_{\alpha_1 \dots \alpha_\ell}^p$  vanishes as  $e^{-d/\xi_l}$ , where  $d$  is the distance from the plaquette  $p$  to the center of the most remote of the LIOMs  $\alpha_1 \dots \alpha_\ell$ .

Next, we note that  $\text{Tr}_k(\hat{n}_{\alpha_1} \dots \hat{n}_{\alpha_\ell}) = \binom{D-\ell}{k-\ell}$ , which is straightforward to verify using combinatorial arguments [note that  $\text{Tr}_k(\hat{n}_{\alpha_1} \dots \hat{n}_{\alpha_\ell}) = 0$  if  $\ell > k$ ]. Using this fact, along with Eq. (11), we find:

$$\text{Tr}_k \bar{m}_p = \sum_{\ell=1}^k \binom{D-\ell}{k-\ell} \sum_{\alpha_1 \dots \alpha_\ell} m_{\alpha_1 \dots \alpha_\ell}^p. \quad (12)$$

Recall from Sec. II.B that  $\text{Tr}_k \bar{m}_p$  a topological invariant for each value of  $k$ , and does not depend on the location of the plaquette  $p$ . Using this fact, an inductive argument (explained below) allows us to identify  $\mu_\ell$  as a topological invariant, where

$$\frac{\mu_\ell}{T} \equiv \sum_{\alpha_1 \dots \alpha_\ell} m_{\alpha_1 \dots \alpha_\ell}^p. \quad (13)$$

Note that  $\mu_\ell$  is independent of the choice of plaquette  $p$ .

To see why  $\mu_\ell$  is a topological invariant, consider setting  $k = 1$  in Eq. (12). In this case, we find  $\sum_\alpha m_\alpha^p = \text{Tr}_1 \bar{m}_p$ . Since  $\text{Tr}_1 \bar{m}_p$  is a topological invariant,  $\mu_1$  is itself a topological invariant. Now set  $k = 2$  in Eq. (12). Using  $\binom{0}{0} = 1$  and  $\binom{a}{1} = a$ , and isolating  $\sum_{\alpha_1 \alpha_2} m_{\alpha_1 \alpha_2}^p$ , we find

$$\sum_{\alpha_1 \alpha_2} m_{\alpha_1 \alpha_2}^p = \text{Tr}_2 \bar{m}_p - (D-1) \frac{\mu_1}{T}. \quad (14)$$

Since both of the terms on the right hand side of Eq. (14) are topological invariants, we conclude that  $\mu_2 = T \sum_{\alpha_1, \alpha_2} m_{\alpha_1 \alpha_2}^p$  must also be a topological invariant. Iterating these arguments, we find  $\mu_\ell$  is a topological invariant for arbitrary  $\ell$ .

Since the magnetization coefficients  $\{m_{\alpha_1 \dots \alpha_\ell}^p\}$  vanish when the distance from any of the LIOM centers  $\mathbf{r}_{\alpha_1} \dots \mathbf{r}_{\alpha_\ell}$  to plaquette  $p$  becomes large, the invariant  $\mu_\ell$  is independent of the size of the system. Thus the invariants  $\{\mu_\ell\}$ , as defined in Eq. (13), characterize the intrinsic topological properties of the system. In essence,  $\mu_\ell$  captures the contribution of  $\ell$ -body correlations to the magnetization density (see below).

#### D. Quantization of $\mu_\ell$

In the above, we established that the sum of magnetization coefficients  $\frac{\mu_\ell}{T} \equiv \sum_{\alpha_1 \dots \alpha_\ell} m_{\alpha_1 \dots \alpha_\ell}^p$  is a topological invariant of the system. Here we show that the value of  $\mu_\ell$  is *quantized* as an integer. The approach we use generalizes that used for the noninteracting case in Ref. 29. This section gives an outline of the arguments, while technical details of the proof are provided in Appendix B. While we for simplicity assume full MBL to be present, we note that the arguments proving the quantization of  $\mu_\ell$  only rely on the localization of Floquet eigenstates consisting of up to  $\ell$  particles.

To establish the quantization of  $\mu_\ell$ , we use the fact that  $\sum_{\alpha_1 \dots \alpha_\ell} m_{\alpha_1 \dots \alpha_\ell}^p$  takes the same value for all plaquettes  $p$  on the lattice. For any given plaquette  $p$ , we may thus compute  $\mu_\ell$  by taking the average value of  $\sum_{\alpha_1 \dots \alpha_\ell} m_{\alpha_1 \dots \alpha_\ell}^p$  over all plaquettes  $p$  in the lattice:

$$\frac{\mu_\ell}{T} = \frac{a^2}{L^2} \sum_p \sum_{\alpha_1 \dots \alpha_\ell} m_{\alpha_1 \dots \alpha_\ell}^p, \quad (15)$$

where  $L^2/a^2$  is the number of plaquettes in the  $L \times L$  lattice, with lattice constant  $a$ .

We now link the sum  $\sum_p m_{\alpha_1 \dots \alpha_k}^p$  to the response of the quasienergy coefficient  $\varepsilon_{\alpha_1 \dots \alpha_k}$  to the insertion of a uniform magnetic field through the system. This relationship is in analogy to non-driven systems, where the magnetic moment of a state gives the response of its energy to a uniform perpendicular magnetic field. To establish this relationship, we encounter a subtlety: the quantization of magnetic flux on closed geometries implies that a uniform magnetic field cannot be continuously varied on the torus (see discussion in the end of Sec. II.A). However, as we show here, the presence of MBL allows for a well-defined notion of the response of the quasienergy  $\varepsilon_{\alpha_1 \dots \alpha_k}$  to a uniform field  $B$ .

Specifically, we consider a Floquet eigenstate  $|\Psi\rangle = |\Psi_{\alpha_1 \dots \alpha_k}\rangle$ , where LIOMs  $\alpha_1 \dots \alpha_k$  are located within a finite disk-shaped region  $R$  of linear dimension  $r$ . We now seek to estimate the response of its quasienergy  $E = E_{\alpha_1 \dots \alpha_k}$  when a uniform magnetic field  $B$  is applied through all plaquettes in the torus, except within a

single plaquette  $q$ , located a distance  $\sim L$  away from  $R$ , where a compensating magnetic flux  $\phi_q = -B(L^2 - a^2)$  is applied. Note that we may vary the field  $B$  continuously, since the configuration of magnetic field results in a zero net flux piercing the torus for any value of  $B$ . Using the spectral decomposition of  $U(T)$ , we find that

$$\frac{\partial E}{\partial B} = \frac{i}{T} \langle \Psi | U^\dagger(T) \frac{\partial}{\partial B} U(T) | \Psi \rangle. \quad (16)$$

Next, explicitly taking the derivative on the right hand side by writing the Floquet operator  $U(T)$  as a time-ordered exponential  $U(T) = \mathcal{T} e^{-i \int_0^T H(t) dt}$ , we find

$$\frac{\partial E}{\partial B} = \frac{1}{T} \int_0^T dt \langle \Psi | U^\dagger(t) \frac{\partial H(t)}{\partial B} U(t) | \Psi \rangle. \quad (17)$$

We identify the right-hand side as the time-averaged expectation value of  $\frac{\partial H(t)}{\partial B}$  in the Floquet eigenstate  $|\Psi\rangle$ , over a single driving period. Since  $|\Psi\rangle$  is a Floquet eigenstate, the average of a ( $T$ -periodic) observable over a single driving period is identical to the long-time averaged value of the observable. Hence

$$\frac{\partial E}{\partial B} = \langle \Psi | \frac{\partial \bar{H}}{\partial B} | \Psi \rangle, \quad (18)$$

where, as in Sec. II,  $\bar{\mathcal{O}}$  denotes the long-time averaged expectation value of the operator  $\mathcal{O}(t)$  in the Heisenberg picture. As a next step, we note that  $\frac{\partial H}{\partial B} = \sum_{p \neq q} \frac{\partial H}{\partial \phi_{pq}}$ , where  $\frac{\partial H}{\partial \phi_{pq}}$  denotes the response of the Hamiltonian to the insertion of a magnetic flux  $\phi_{pq}$  through plaquette  $p$ , while a compensating flux is inserted through plaquette  $q$  (see Sec. II.A.1). Thus, using Eq. (8), we find

$$\frac{\partial E}{\partial B} = \sum_p a^2 \langle \Psi | \bar{m}_p | \Psi \rangle - L^2 \langle \Psi | \bar{m}_q | \Psi \rangle. \quad (19)$$

We finally recall that plaquette  $q$  is located a distance  $\sim L$  from the region of support of the Floquet eigenstate  $|\Psi\rangle$ . Hence  $\langle \Psi | \bar{m}_q | \Psi \rangle \sim \mathcal{O}(e^{-L/\xi_t})$ . Restoring the indices  $\alpha_1 \dots \alpha_k$ , we thus obtain, in the thermodynamic limit

$$\frac{\partial E_{\alpha_1 \dots \alpha_k}}{\partial B} = \sum_p a^2 \langle \Psi_{\alpha_1 \dots \alpha_k} | \bar{m}_p | \Psi_{\alpha_1 \dots \alpha_k} \rangle. \quad (20)$$

Next, we expand  $E_{\alpha_1 \dots \alpha_k}$  in terms of the quasienergy coefficients  $\{\varepsilon_{\alpha_1 \dots \alpha_k}\}$ , and expand the expectation value on the right-hand side in terms of the magnetization coefficients  $\{m_{\alpha_1 \dots \alpha_k}^p\}$ . Comparing the expansions for different values of  $\ell$ , one can verify

$$\frac{\partial \varepsilon_{\alpha_1 \dots \alpha_\ell}}{\partial B} = -a^2 \sum_p m_{\alpha_1 \dots \alpha_\ell}^p. \quad (21)$$

As a next crucial step, we approximate the derivative  $\partial \varepsilon_{\alpha_1 \dots \alpha_\ell} / \partial B$  from the finite response of the quasienergy coefficient  $\varepsilon_{\alpha_1 \dots \alpha_\ell}$  to the insertion of a weak uniform field

through the *full* system, with magnitude  $B_0 = \frac{2\pi}{L^2}$  corresponding to precisely one flux quantum piercing the torus. This relation is nontrivial due to the exponentially small level spacing in the system, and is proven in Appendix B. Here we sketch the arguments, which proceed in two steps.

First we show that, even though the system's quasienergy spectrum exhibits exponentially many avoided crossings under a continuous perturbation, the eigenstates and quasienergies in the presence of the field  $B_0$  are approximately identical to those of the system in the absence of the field  $B_0$  (for all but a measure zero set of disorder realizations). Specifically, we let  $\{|\tilde{\Psi}_{\alpha_1 \dots \alpha_k}\rangle\}$  denote the  $k$ -particle Floquet eigenstates of the system in the presence of the uniform field  $B_0$ . In Appendix B, we show that, with a probability that goes to 1 in the thermodynamic limit (and for any finite value of the particle number,  $k$ ), it is possible to label the complete set of Floquet eigenstates  $\{|\tilde{\Psi}_{\alpha_1 \dots \alpha_k}\rangle\}$  such that, for *each* choice of the LIOM indices  $\alpha_1 \dots \alpha_k$ ,  $|\tilde{\Psi}_{\alpha_1 \dots \alpha_k}\rangle = |\Psi_{\alpha_1 \dots \alpha_k}\rangle$ , up to a gauge transformation and a correction that vanishes in the thermodynamic limit.

As a second key step, we show that each quasienergy coefficient  $\tilde{\varepsilon}_{\alpha_1 \dots \alpha_\ell}$  deviates from  $\varepsilon_{\alpha_1 \dots \alpha_\ell}$  by a small amount controlled by  $B_0 \sum_p a^2 m_{\alpha_1 \dots \alpha_\ell}^p$ . Specifically [see Appendix B], we find, in the thermodynamic limit,

$$\frac{\tilde{\varepsilon}_{\alpha_1 \dots \alpha_\ell} - \varepsilon_{\alpha_1 \dots \alpha_\ell}}{B_0} = a^2 \sum_p m_{\alpha_1 \dots \alpha_\ell}^p. \quad (22)$$

Comparing with Eq. (21), we confirm that the derivative  $\partial \varepsilon_{\alpha_1 \dots \alpha_\ell} / \partial B$  is well-approximated by the finite response  $(\tilde{\varepsilon}_{\alpha_1 \dots \alpha_\ell} - \varepsilon_{\alpha_1 \dots \alpha_\ell}) / B_0$ .

To link the above result with the invariant  $\mu_\ell$ , we sum Eq. (22) over all combinations of the indices  $\alpha_1 \dots \alpha_\ell$ . Using  $B_0 = 2\pi/L^2$ , along with Eq. (15), we obtain

$$\frac{\mu_\ell}{T} = \frac{1}{2\pi} \sum_{\alpha_1 \dots \alpha_\ell} (\tilde{\varepsilon}_{\alpha_1 \dots \alpha_\ell} - \varepsilon_{\alpha_1 \dots \alpha_\ell}). \quad (23)$$

Next we relate the sum on the right hand side of Eq. (23) to the determinants of the Floquet operators  $\tilde{U}(T)$  and  $U(T)$  of the one- and zero-flux systems, respectively. Letting  $|\mathcal{O}|_k$  denote the determinant of the operator  $\mathcal{O}$  within the  $k$ -particle subspace, we find that

$$\frac{|\tilde{U}(T)|_k}{|U(T)|_k} = e^{-i \sum_{\alpha_1 \dots \alpha_k} (\tilde{E}_{\alpha_1 \dots \alpha_k} - E_{\alpha_1 \dots \alpha_k}) T}. \quad (24)$$

Crucially, the determinants  $|\tilde{U}|_k$  and  $|U|_k$  must be identical. To see this, note that the determinant of any time-evolution operator can be found from the time-averaged trace of the Hamiltonian:  $|U(T)|_k = e^{-i \int_0^T dt' \text{Tr}_k H(t')}$  (for a proof, see, e.g., Ref. 16). Since the insertion of a magnetic flux only modifies off-diagonal elements of the Hamiltonian (in position space), the trace of the Hamiltonian is unaffected by the magnetic field  $B_0$ . We thus conclude  $|\tilde{U}(T)|_k = |U(T)|_k$ . The right-hand side of Eq. (24)

must therefore be equal to 1. This implies that

$$\sum_{\alpha_1 \dots \alpha_k} (\tilde{E}_{\alpha_1 \dots \alpha_k} - E_{\alpha_1 \dots \alpha_k}) = \frac{2\pi z_\ell}{T}, \quad (25)$$

for some integer  $z_\ell$ . Using an inductive argument similar to the one made below Eq. (13), one can show that the above result implies that, for each  $\ell$ ,

$$\sum_{\alpha_1 \dots \alpha_\ell} (\tilde{\varepsilon}_{\alpha_1 \dots \alpha_\ell} - \varepsilon_{\alpha_1 \dots \alpha_\ell}) = \frac{2\pi z'_\ell}{T}, \quad (26)$$

for some (different) integer  $z'_\ell$ . Comparing with Eq. (23), we conclude that  $\mu_\ell$  is quantized as an integer.

### E. Quantized magnetization density in fully occupied regions

Here we show that the values of the invariants  $\{\mu_\ell\}$  can be measured directly from the magnetization density within a region of the system where all sites are occupied.

Consider preparing the system in a state  $|\Psi_{\mathcal{R}}\rangle$  by filling all sites in some finite region of the lattice,  $\mathcal{R}$ , of linear dimension  $d$ , with all sites outside  $\mathcal{R}$  remaining empty. For a plaquette  $p$  located deep within the fully occupied region, we find the time-averaged magnetization density as  $\langle\langle m_p \rangle\rangle = \langle\bar{m}_p\rangle_{\mathcal{R}}$ , where we introduced the shorthand  $\langle\mathcal{O}\rangle_{\mathcal{R}} \equiv \langle\Psi_{\mathcal{R}}|\mathcal{O}|\Psi_{\mathcal{R}}\rangle$ . Using the expansion of  $\bar{m}_p$  in Eq. (11), we thus find:

$$\langle\langle m_p \rangle\rangle = \sum_{\alpha_1} m_{\alpha_1}^p \langle\hat{n}_{\alpha_1}\rangle_{\mathcal{R}} + \sum_{\alpha_1 \alpha_2} m_{\alpha_1 \alpha_2}^p \langle\hat{n}_{\alpha_1} \hat{n}_{\alpha_2}\rangle_{\mathcal{R}} + \dots \quad (27)$$

To analyze the sum, we note that, for a LIOM  $\hat{n}_a$  whose center  $\mathbf{r}_a$  is located deep within the filled region  $\mathcal{R}$ , all sites where  $\hat{n}_a$  has its support are occupied. Thus<sup>51</sup>  $\hat{n}_a|\Psi_{\mathcal{R}}\rangle = |\Psi_{\mathcal{R}}\rangle + \mathcal{O}(e^{-d/\xi_l})$ . Here the correction arises from the exponentially decaying tail of  $\hat{n}_a$  outside the filled region. For terms in the above equation where the centers of all the LIOMs  $\alpha_1 \dots \alpha_\ell$  are located near the plaquette  $p$ , the above result implies that  $\langle\hat{n}_{\alpha_1} \dots \hat{n}_{\alpha_\ell}\rangle_{\mathcal{R}} = 1 + \mathcal{O}(e^{-d/\xi_l})$ , since *all* of the LIOMs  $\hat{n}_{\alpha_1} \dots \hat{n}_{\alpha_\ell}$  are located deep within the initially occupied region. For all remaining terms in Eq. (27), one or more LIOMs  $\alpha_1 \dots \alpha_\ell$  are located outside the filled region, and thus reside at least a distance  $\sim d$  from the plaquette  $p$ . In this case, the coefficient  $m_{\alpha_1 \dots \alpha_\ell}^p$  is exponentially small in  $d/\xi_l$  [see the discussion below Eq. (11)]. For both categories of terms we can thus set  $\langle\Psi_{\mathcal{R}}|m_{\alpha_1 \dots \alpha_\ell}^p \hat{n}_{\alpha_1} \dots \hat{n}_{\alpha_\ell}|\Psi_{\mathcal{R}}\rangle = m_{\alpha_1 \dots \alpha_\ell}^p$ , at the cost of a correction of order  $e^{-d/\xi_l}$ . Doing so, we obtain

$$\langle\langle m_p \rangle\rangle = \sum_{\alpha_1} m_{\alpha_1}^p + \sum_{\alpha_1 \alpha_2} m_{\alpha_1 \alpha_2}^p + \dots + \mathcal{O}(e^{-d/\xi_l}).$$

Using Eq. (13), we identify the  $\ell$ -th sum above as the invariant  $\mu_\ell/T$ . Recalling that  $\langle\Psi_{\mathcal{R}}|\bar{m}_p|\Psi_{\mathcal{R}}\rangle = \langle\langle m_p \rangle\rangle$ ,



we thus find:

$$\langle\langle m_p \rangle\rangle = \frac{1}{T} \sum_{\ell=1}^{\infty} \mu_{\ell} + \mathcal{O}(e^{-d/\xi_l}). \quad (28)$$

The above discussion thus shows that the magnetization density deep within the filled region is given by the (convergent<sup>52</sup>) sum of the invariants  $\{\mu_{\ell}\}$ .

We note that the individual invariants  $\mu_{\ell}$  may be extracted from the dependence of the magnetization density on the particle density in the system. Specifically, for a random initial state with a uniform, finite particle density  $\rho$ , the expectation value  $\langle \hat{n}_{\alpha_1} \dots \hat{n}_{\alpha_{\ell}} \rangle$ , averaged over all choices of LIOMs, is given by  $\rho^{\ell}$ . Hence, at finite particle density  $\rho$ , the average magnetization density in the system is given by  $\langle\langle m_p \rangle\rangle \approx \frac{1}{T} \sum_{\ell=1}^{\infty} \mu_{\ell} \rho^{\ell}$ . The values of the individual invariants  $\mu_{\ell}$  can thus be extracted from a fit of  $\langle\langle m_p \rangle\rangle$  as a function of  $\rho$ .

### III. NATURE OF HIGHER-ORDER INVARIANTS

Above, we found that there is not one, but in fact a whole family of AFI phases characterized by the topological invariants  $\{\mu_{\ell}\}$ . In this subsection, we briefly discuss the nature of this family.

The invariant  $\mu_{\ell}$  is computed from the terms in the expansion (11) that involve products of  $\ell$  LIOMs. Thus  $\mu_{\ell}$  encodes information about the  $\ell$ -body correlations of the system. In the absence of interactions, and assuming the absence of correlations in the initial state, the evolution of the system is described by a Slater-determinant of time-evolved single particle states. In this case, correlations between two or more particles are absent for all times, and we must have  $m_{\alpha_1 \dots \alpha_{\ell}}^p = 0$  for  $\ell \geq 2$ . Therefore, only the invariant  $\mu_1$  may be nonzero when interactions are absent. When  $\mu_1 \neq 0$ , the system is in the AFAI phase<sup>9,29,30</sup> and we identify  $\mu_1$  with the “winding number” invariant that characterizes this phase.

The arguments at the end of Sec. II show that the invariant  $\mu_{\ell}$  cannot change under smooth deformations that maintain the localization of all Floquet eigenstates with  $\ell$  particles or less. Hence, the “higher” invariants  $\mu_2, \mu_3, \dots$  must all take the value zero for an AFI that can be smoothly connected to the noninteracting AFAI without breaking MBL (for instance if the Hamiltonian of the AFI is constructed by adding weak interactions to an AFAI). However, it is possible for the higher invariants to be nonzero. A system characterized by nonzero values of one or more of the invariants  $\mu_2, \mu_3, \dots$  will be in a new, strongly-correlated non-equilibrium phase that cannot exist in the absence of interactions. Below we demonstrate that a nonzero value of the invariant  $\mu_2$  can be realized in a model with correlated hopping. A more detailed study of the nature of these additional invariants is beyond the scope of this work, but presents an interesting direction for future studies.

We note that the topological protection of the invariant  $\mu_{\ell}$  does not require full many-body localization. While the discussion above for simplicity assumed the system to be MBL, the arguments proving the topological invariance and quantization of  $\mu_{\ell}$  only rely on Floquet eigenstates with  $\ell$  particles or less being localized<sup>53</sup>. In this way, the topological robustness of the system relies on *partial localization* (i.e., localization of the system when restricted to sectors with up to  $\ell$  particles, where  $\ell$  is finite). In particular, if all Floquet eigenstates with  $\ell_0$  particles or less are localized, the system is characterized by the  $\ell_0$  topological invariants  $\mu_1, \dots, \mu_{\ell_0}$ . Each invariant  $\mu_{\ell}$  can only change its value at a phase transition where the Floquet eigenstates with  $\ell$  particles or fewer become delocalized (in an infinitely large system).

#### A. Model with nontrivial value of $\mu_2$

In this subsection, we explicitly demonstrate that a nontrivial value of the invariant  $\mu_2$  can be realized in a model with correlated hopping. The model we consider is a modified version of the AFI model studied in Ref. 38 (see also Sec. IV below). The system consists of interacting spin-1/2 fermions on a bipartite square lattice of dimensions  $L \times L$  on a torus, with lattice constant  $a$ . The Hamiltonian of the system  $H(t)$  consists of piecewise-constant, time-dependent correlated hopping terms. The driving protocol is divided into four segments, each of duration  $T/4$ . Within the  $j$ -th segment,  $H(t)$  is given by the Hamiltonian  $H_j$ , where

$$H_j = \frac{2\pi}{T} \sum_{\mathbf{r} \in A} \sum_{s=\uparrow, \downarrow} \hat{\Gamma}_{\mathbf{r}+\mathbf{b}_j} \hat{\Gamma}_{\mathbf{r}} (\hat{c}_{\mathbf{r}+\mathbf{b}_j, s}^{\dagger} \hat{c}_{\mathbf{r}, s} + \text{h.c.}) \hat{\Gamma}_{\mathbf{r}} \hat{\Gamma}_{\mathbf{r}+\mathbf{b}_j}. \quad (29)$$

Here  $\hat{c}_{\mathbf{r}, s}$  annihilates a fermion on site  $\mathbf{r}$  with spin  $s$ , and the vectors  $\{\mathbf{b}_j\}$  are given by  $\mathbf{b}_1 = -\mathbf{b}_3 = (a, 0)$  and  $\mathbf{b}_2 = -\mathbf{b}_4 = (0, a)$ . The  $\mathbf{r}$ -sum above runs over all sites in sublattice A of the bipartite square lattice. Finally, the operator  $\hat{\Gamma}_{\mathbf{r}}$  is defined as  $\hat{\Gamma}_{\mathbf{r}} \equiv (1 - \hat{\rho}_{\mathbf{r}, \uparrow} \hat{\rho}_{\mathbf{r}, \downarrow})$ , where  $\hat{\rho}_{\mathbf{r}, s} \equiv \hat{c}_{\mathbf{r}, s}^{\dagger} \hat{c}_{\mathbf{r}, s}$  measures the occupancy of particles on site  $\mathbf{r}$  with spin  $s$ . Thus,  $\hat{\Gamma}_{\mathbf{r}}|\Psi\rangle = 0$  when two fermions occupy site  $\mathbf{r}$  in the state  $|\Psi\rangle$ , while  $\hat{\Gamma}_{\mathbf{r}}|\Psi\rangle = |\Psi\rangle$ , if site  $\mathbf{r}$  is occupied by zero or one fermion.

As defined above,  $H_j$  describes hopping on bonds between sites  $\mathbf{r}$  and  $\mathbf{r} + \mathbf{b}_j$  (for each site  $\mathbf{r}$  in sublattice A) whenever the two coupled sites together hold only one fermion. The tunneling strength of  $2\pi/T$  ensures that a particle located on site  $\mathbf{r}$  is perfectly transferred to the site  $\mathbf{r} + \mathbf{b}_j$  in the  $j$ -th segment (and vice versa) if hopping is allowed. If the sites  $\mathbf{r}$  and  $\mathbf{r} + \mathbf{b}_j$  together hold two or more particles,  $H_j$  acts trivially on the sites. In this case, the configuration of particles on sites  $\mathbf{r}$  and  $\mathbf{r} + \mathbf{b}_j$  does not change in segment  $j$ .

With the tunneling strength set to  $2\pi/T$ , the model is exactly solvable; away from this point, disorder would be needed to stabilize the evolution. In Appendix C we give a detailed analysis of the dynamics of the solvable model



and identify its Floquet eigenstates in the subspaces with 1 and 2 particles (see below).

We study the topology of the model by inferring the values of the invariants  $\{\mu_\ell\}$  from the magnetic moments of the system's Floquet eigenstates. Here the magnetic moment operator is defined as  $\bar{M} \equiv \sum_p a^2 \bar{m}_p$ . From Eq. (21), we see that this operator measures the response of a Floquet eigenstate's quasienergy to the introduction of a uniform magnetic field in the region where the particle density is nonzero. Using Eqs. (12)-(13) along with Eq. (10), we can relate the trace of  $\bar{M}$  to the invariants  $\{\mu_\ell\}$  as follows:

$$\text{Tr}_k \bar{M} = \frac{L^2}{T} \sum_{\ell=1}^k \binom{D-\ell}{k-\ell} \mu_\ell, \quad (30)$$

where  $L^2 \equiv \sum_p a^2$  denotes the area of the system. The above result allows us to infer the value of the invariant  $\mu_\ell$  from the trace  $\text{Tr}_k \bar{M}$ , along with the “lower-order” invariants  $\mu_1 \dots \mu_{\ell-1}$ .

In the single-particle subspace, we may ignore interactions, and set  $\hat{\Gamma}_r = 1$ . Thus, the mode's single-particle dynamics are described by the solvable AFAI model in Ref. 9. Analogous to Ref. 9, the single-site-localized states (of either spin projection) form a basis of Floquet eigenstates; each state in this case sweeps out one plaquette per driving period. In the presence of a uniform magnetic field  $B$ , the state picks up a phase of  $Ba^2$  as the particle traverses the plaquette, corresponding to a shift in the state's quasienergy of  $\Delta\varepsilon = Ba^2/T$ . Hence the magnetic moment of each single particle Floquet eigenstate is  $a^2/T$ . Since there are  $2L^2/a^2$  Floquet eigenstates in total (where the factor of 2 arises from the spin degeneracy), we find that  $\text{Tr}_1 \bar{M} = 2L^2/T$ . Using Eq. (30) along with Eqs. (12)-(13), we conclude that  $\mu_1 = 2$ .

For the two-particle subspace, the  $\hat{\Gamma}_r$  factors can be ignored for Floquet eigenstates where the two particles are separated by a large distance. For such two-particle Floquet eigenstates, the particles collectively (and independently) sweep out two plaquettes per driving period; hence the magnetic moment of each of these states is given by  $2a^2/T$ . The only Floquet eigenstates that do not sweep out two plaquettes per period are Floquet eigenstates where a site is occupied by two fermions: the Hamiltonian  $H(t)$  acts trivially on these states, and the particles remain confined to the same site throughout the driving period. These Floquet eigenstates therefore have zero magnetic moment. These considerations show that there are  $D = L^2/a^2$  Floquet eigenstates with magnetic moment 0, while all remaining 2-particle Floquet eigenstates have magnetic moment  $2a^2/T$ . Thus the sum of magnetic moments over all Floquet eigenstates takes a *smaller* value than if there were no interactions, where the magnetic moment of *each* Floquet eigenstate would be given by  $2a^2/T$ . Since  $\mu_2 = 0$  in the noninteracting case, we thus conclude that  $\mu_2 < 0$  for the model we study here. Indeed, as we show explicitly in Appendix C,  $\mu_2 = -2$ . Hence the model presented in this subsec-

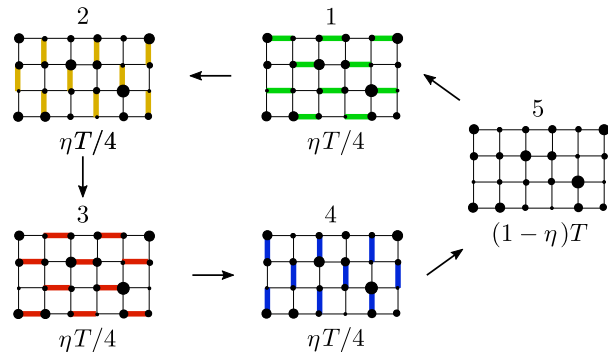


FIG. 3. Schematic depiction of the model studied in Sec. IV (see main text for details).

tion realizes a phase which is topologically distinct from the non-interacting AFAI. A similar approach may also be used to calculate the values of the higher-order invariants ( $\mu_\ell$  for  $\ell \geq 3$ ). We expect these invariants to also be nonzero.

In this section we demonstrated that it is possible for “higher-order” invariants  $\mu_\ell$  for  $\ell \geq 2$  to be nonzero. Specifically, the model in Eq. (29) is characterized by a nonzero, quantized value of the invariant  $\mu_2$ . Although the quantization of  $\mu_2$  for this particular model appears to be the result of fine-tuning to the special point where the Hamiltonian generates perfect “ $\pi$ -pulses” in each segment, we emphasize that the index is topologically robust: the discussion in Sec. II shows that  $\mu_2$  remains a quantized invariant under perturbations that preserve localization within the one- and two-particle subspaces.

It is not presently clear if the model above is many-body localized in the thermodynamic limit, or if nonzero values of the “higher” invariants  $\mu_2, \dots$  are compatible with MBL. In particular, for the model studied here, consider an initial state where each site in some large region  $\mathcal{R}$  is initially occupied by two particles, while sites surrounding  $\mathcal{R}$  are occupied by one or zero particles. Due to blocked hopping from doubly-occupied sites, the particles within  $\mathcal{R}$  remain inert at all times. For the remaining particles outside region  $\mathcal{R}$ , the blocked hopping to sites within  $\mathcal{R}$  results in the formation of a chiral edge state around  $\mathcal{R}$ . The proliferation of such chiral edge states could potentially lead to thermalization in the system. The existence of MBL in this model (and other model with nonzero values of the higher invariants) is therefore not clear, but may be an interesting direction of future studies.

#### IV. NUMERICAL SIMULATIONS

To support the main conclusions of Sec. II, we numerically investigate the magnetization density of a finite droplet of particles in a disordered, interacting, periodically-driven system. We simulate the dynamics of interacting spinless fermions on a two-dimensional

bipartite square lattice with periodic boundary conditions. The Hamiltonian we study is given by  $H(t) = H_{\text{dr}}(t) + H_{\text{dis}} + H_{\text{int}}$ , where  $H_{\text{dr}}(t)$  describes piecewise-constant, time-dependent hopping, while  $H_{\text{dis}}$  and  $H_{\text{int}}$  are time-independent disorder and interaction potentials.

The driving protocol, which is contained in  $H_{\text{dr}}(t)$ , is divided into five segments, as depicted in Fig. 3. The first four segments each have duration  $\eta T/4$ , while the fifth segment has duration  $(1-\eta)T$ ; the parameter  $\eta$  is a number between 0 and 1 which controls the localization properties of the model (see below). In the first four segments,  $H_{\text{dr}}(t)$  turns hopping on for the four different bond types in a counterclockwise fashion, as indicated in Fig. 3, while  $H_{\text{dr}}(t) = 0$  in the fifth segment. More specifically, in the  $j$ -th segment (where  $j \leq 4$ ),

$$H_{\text{dr}}(t) = J \sum_{\mathbf{r} \in A} (\hat{c}_{\mathbf{r}+\mathbf{b}_j}^\dagger \hat{c}_{\mathbf{r}} + \text{h.c.}). \quad (31)$$

Here the vectors  $\{\mathbf{b}_j\}$  are as given for the correlated hopping model in Sec. III.A [see text below Eq. (29)]. We set the tunneling strength to  $J = \frac{2\pi}{\eta T}$ , such that  $H_{\text{dr}}$  generates a perfect transfer of particles in each of the first four segments (in the absence of disorder and interactions). The parameter  $\eta$  controls how rapidly the “hopping  $\pi$ -pulses” are applied (and thereby how strong they are), and thus controls the localization properties of the model; smaller  $\eta$  yields stronger localization.

The time-independent disorder and interaction terms  $H_{\text{dis}}$  and  $H_{\text{int}}$  are given by

$$H_{\text{dis}} = \sum_{\mathbf{r}} w_{\mathbf{r}} \hat{\rho}_{\mathbf{r}}, \quad H_{\text{int}} = V \sum_{\langle \mathbf{r}\mathbf{r}' \rangle} \hat{\rho}_{\mathbf{r}} \hat{\rho}_{\mathbf{r}'}. \quad (32)$$

For each site,  $w_{\mathbf{r}}$  takes a random value in the interval  $[-W, W]$ , and  $\hat{\rho}_{\mathbf{r}} \equiv \hat{c}_{\mathbf{r}}^\dagger \hat{c}_{\mathbf{r}}$  denotes the occupancy on site  $\mathbf{r}$ . The parameter  $V$  has units of energy and denotes the strength of the interactions.

The model above was used in Ref. 38 to study the compatibility of the AFI with MBL. There, the system was found to remain stable (i.e. non-thermalizing) on all numerically accessible time-scales in the regime where  $1/\eta T \gg W \gg V$ . In this section, we study the topological properties of the model in the same regime. We consider a single disorder realization of the model, with 5 particles on a lattice of  $7 \times 8$  sites with periodic boundary conditions. The parameters we use for the model are set to  $W = 2\pi/T$ ,  $V = 0.1W$ , and  $\eta = 1/16$ , which, following the results in Ref. 38, brings the model into the localized regime. Since the model is obtained by adding weak interactions to a model of the AFAI with winding number 1 (see Refs. 29 and 30), we expect  $\mu_1$  to be given by 1 for the model, while  $\mu_\ell = 0$  for all other values of  $\ell$  (see the discussion in Sec. III).

To probe the topology of the system, we compute the mean magnetic moments of random time-evolved 5-particle states. The long-time averaged magnetic moment, introduced in Sec. III, is defined as  $\bar{M} = \sum_p a^2 \bar{m}_p$ .

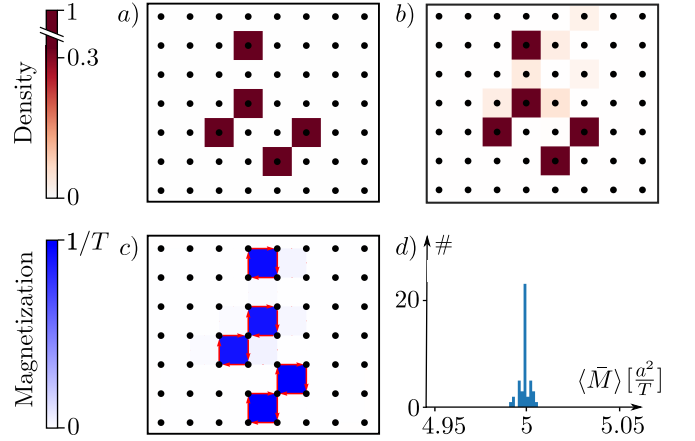


FIG. 4. Particle density and magnetization density in the model studied in Sec. IV, when initialized in a random state of 5 particles localized on sites of a  $7 \times 8$  lattice. Parameter values:  $\eta = 1/16$ ,  $W = 2\pi/T$ ,  $V = 0.5W$ . a) Initial particle density. b) Final particle density after the state in panel a has been evolved for 5000 driving periods. c) Time-averaged magnetization density (blue) and bond-currents (red) after the initialization depicted in panels a has been evolved for 5000 periods. d) Histogram of magnetic moments of 45 randomly chosen initial states that are evolved for 5000 periods (see main text for details).

The mean expectation value of  $\bar{M}$ , averaged over randomly chosen  $k$ -particle states (i.e., states chosen randomly from a given orthonormal basis) is given by  $M_0 \equiv \binom{D}{k}^{-1} \text{Tr}_k \bar{M}$ , where the binomial coefficient  $\binom{D}{k}$  counts the number of possible  $k$ -particle states in the system of  $D$  sites. Using Eq. (30), we can express the mean value  $M_0$  in terms of the topological invariants  $\{\mu_\ell\}$ :  $M_0 = \frac{a^2}{T} \sum_\ell A_\ell \mu_\ell$ , where  $A_\ell = D \binom{D-\ell}{k-\ell} / \binom{D}{\ell}$ . For  $k = 5$  particles on a  $7 \times 8$  lattice of  $D = 56$  sites, we find:

$$M_0 \approx (5\mu_1 + 0.36\mu_2 + 0.02\mu_3 + 0.0007\mu_4 + 0.00001\mu_5) \frac{a^2}{T}.$$

Using this relation, we may infer the values of the invariants  $\mu_1 \dots \mu_4$  from the mean magnetic moment of all 5-particle states in the system,  $M_0$ .

To estimate  $M_0$ , we pick 45 random configurations of particles located on individual sites as initial states, and evolve each for 5000 driving periods with a fixed disorder realization (the same for all initial states). Fig. 4a shows the initial particle density for one of the initializations, while Fig. 4b shows the particle density in the resulting final state after evolution for 5000 periods. Fig. 4c shows the time-averaged bond currents and magnetization density in the system for the same state. We compute the time-averaged magnetic moment  $\langle \bar{M} \rangle$  for each of the 45 states, using the time-averaged bond-currents. The 45 values of  $\langle \bar{M} \rangle$  we obtained in this way are plotted in the histogram in Fig. 4d. The distribution of  $\langle \bar{M} \rangle$  obtained from these initializations was found to have mean  $5.0012 a^2/T$  and standard deviation  $0.0029 a^2/T$ . We

thus infer<sup>54</sup>  $M_0 = (5.0012 \pm 0.0004)a^2/T$ . This result is consistent with  $\mu_1 = 1$  while  $\mu_2 = \mu_3 = \mu_4 = \mu_5 = 0$ .

## V. DISCUSSION

In this paper, we studied the topological properties of two-dimensional anomalous Floquet insulators. We identified a family of topological invariants that are encoded in the time-averaged magnetization density operator, and which characterize these phases. Importantly, the nontrivial topological properties of the system do not rely on full many-body localization, but rather on *partial localization*, where the system is localized for any finite number of particles up to a maximum number,  $\ell_0$ . Since the existence of the invariants does not rely on full many-body localization, they may lead to experimental signatures in the prethermal dynamics of systems which eventually thermalize at long times. Searching for other models that give rise to nontrivial values of these invariants and characterizing the physical properties that they imply will be interesting directions for future studies.

Above we focused on driven fermionic models and their bulk topological invariants. Chiral phases of spins and bosons, which are close relatives of the AFAI (with higher-order invariants being zero,  $\mu_\ell = 0$ ,  $\ell > 2$ ), were considered in Ref. 28. It was shown that such phases are characterized by a quantized topological index which describes the pumping of quantum information along the edge over one driving period. Such an index arises from the rigorous classification of anomalous local unitary operators in one-dimensional systems, developed by Gross et al<sup>55</sup>.

In future work, it would be interesting to explore a possible relation between the quantized magnetization (bulk invariant) studied above and the edge index of Refs. 28 and 55. As noted in Refs. 28 and 56, the simplest version of a fermionic AFI is likely topologically equivalent to its bosonic counterpart, which hints that adapting the approach developed above to bosonic/spin systems may be possible. However, it appears that AFI phases with higher-order invariants being non-zero ( $\mu_\ell \neq 0$  for some  $\ell \geq 2$ ) are not captured by the classification of Refs. 28 and 56. Since the edge behavior of such phases depends crucially on the filling of the bulk states, it is not a priori clear whether edge topological indices may

be defined in this case. We leave a detailed study of the edge states and bulk-edge correspondence in such “higher-order” AFI phases as an interesting open question.

We further anticipate that the higher-order AFI phases will exhibit dynamics that strongly depends on the initial state, as suggested by the discussion at the end of Sec. III. In the model of Sec. III.A, initial states where some large region  $\mathcal{R}$  is fully filled would support chiral edge states moving around such regions. If the initial state contains such “internal edges,” they may thermalize and serve as a weak heat bath for the remainder of the system. Next, if the density of filled regions  $\mathcal{R}$  in the system is increased, we expect that at some point thermalizing internal edges will form a connected network, destroying localization. In contrast, initial states without fully-filled connected regions are expected to be much more stable, since there are no direct thermalization processes which involve few nearby particles; thermalization, if occurs at all, will proceed either due to rare thermal inclusions, or due to multi-particle tunneling into, e.g., a state with internal edges.

In the future, it will be interesting to investigate how the above processes are manifested in experimentally realistic situations, and what are the corresponding time scales. It is natural to expect that thermalization will be parametrically slow, and therefore signatures of the AFI (such as quantization of magnetization) would be observable even if MBL is eventually destroyed. Finally, we note that the above discussion suggests that AFI phases may provide a versatile playground for studying the interplay of weak thermalizing baths and MBL regions, which is expected to give new insights into the stability of MBL in 2d.

## VI. ACKNOWLEDGEMENTS

M.R. and F.N. thank the Villum Foundation for support. D.A. acknowledges support by the Swiss National Science Foundation. N.L. acknowledges support from the European Research Council (ERC) under the European Union Horizon 2020 Research and Innovation Programme (Grant Agreement No. 639172), and from the Israeli Center of Research Excellence (I-CORE) “Circle of Light”. M.R. and E.B. acknowledge support from CRC 183 of the Deutsche Forschungsgemeinschaft.

<sup>1</sup> W. Yao, A. H. MacDonald, and Q. Niu, Physical Review Letters **99**, 047401 (2007).

<sup>2</sup> T. Oka and H. Aoki, Phys. Rev. B **79**, 081406 (2009).

<sup>3</sup> T. Kitagawa, E. Berg, M. Rudner, and E. Demler, Phys. Rev. B **82**, 235114 (2010).

<sup>4</sup> J.-I. Inoue and A. Tanaka, Physical Review Letters **105**, 017401 (2010).

<sup>5</sup> N. H. Lindner, G. Refael, and V. Galitski, Nat. Phys. **7**,

490 (2011).

<sup>6</sup> T. Kitagawa, T. Oka, A. Brataas, L. Fu, and E. Demler, Phys. Rev. B **84**, 235108 (2011).

<sup>7</sup> Z. Gu, H. A. Fertig, D. P. Arovas, and A. Auerbach, Physical Review Letters **107**, 216601 (2011).

<sup>8</sup> L. Jiang, T. Kitagawa, J. Alicea, A. R. Akhmerov, D. Pekker, G. Refael, J. I. Cirac, E. Demler, M. D. Lukin, and P. Zoller, Phys. Rev. Lett. **106**, 220402 (2011).

- <sup>9</sup> M. S. Rudner, N. H. Lindner, E. Berg, and M. Levin, Phys. Rev. X **3**, 031005 (2013).
- <sup>10</sup> P. Delplace, A. Gomez-Leon, and G. Platero, Phys. Rev. B **88**, 245422 (2013).
- <sup>11</sup> Y. T. Katan and D. Podolsky, Physical Review Letters **110**, 016802 (2013).
- <sup>12</sup> G. Usaj, P. M. Perez-Piskunow, L. E. F. Foa Torres, and C. A. Balseiro, Physical Review B **90**, 115423 (2014).
- <sup>13</sup> J. K. Asboth, B. Tarasinski, and P. Delplace, Phys. Rev. B **90**, 125143 (2014).
- <sup>14</sup> G. Jotzu, M. Messer, R. Desbuquois, M. Lebrat, T. Uehlinger, D. Greif, and T. Esslinger, Nature **515**, 237 (2014).
- <sup>15</sup> D. Carpentier, P. Delplace, M. Fruchart, and K. Gawedzki, Phys. Rev. Lett. **114**, 106806 (2015).
- <sup>16</sup> F. Nathan and M. S. Rudner, New Journal of Physics **17**, 125014 (2015).
- <sup>17</sup> R. Roy and F. Harper, Phys. Rev. B **96**, 155118 (2017).
- <sup>18</sup> D. V. Else and C. Nayak, Physical Review B **93**, 201103 (2016).
- <sup>19</sup> R. Roy and F. Harper, Physical Review B **94**, 125105 (2016).
- <sup>20</sup> C. W. von Keyserlingk and S. L. Sondhi, Phys. Rev. B **93**, 245145 (2016).
- <sup>21</sup> C. W. von Keyserlingk and S. L. Sondhi, Phys. Rev. B **93**, 245146 (2016).
- <sup>22</sup> C. W. von Keyserlingk, V. Khemani, and S. L. Sondhi, Phys. Rev. B **94**, 085112 (2016).
- <sup>23</sup> A. C. Potter, T. Morimoto, and A. Vishwanath, Phys. Rev. X **6**, 041001 (2016).
- <sup>24</sup> V. Khemani, A. Lazarides, R. Moessner, and S. L. Sondhi, Phys. Rev. Lett. **116**, 250401 (2016).
- <sup>25</sup> D. V. Else, B. Bauer, and C. Nayak, Phys. Rev. Lett. **117**, 090402 (2016).
- <sup>26</sup> S. Choi, J. Choi, R. Landig, G. Kucsko, H. Zhou, J. Isoya, F. Jelezko, S. Onoda, H. Sumiya, V. Khemani, et al., Nature **543**, 221 (2017).
- <sup>27</sup> J. Zhang, P. W. Hess, A. Kyprianidis, P. Becker, A. Lee, J. Smith, G. Pagano, I.-D. Potirniche, A. C. Potter, A. Vishwanath, et al., Nature **543**, 217 (2017).
- <sup>28</sup> H. C. Po, L. Fidkowski, T. Morimoto, A. C. Potter, and A. Vishwanath, Phys. Rev. X **6**, 041070 (2016).
- <sup>29</sup> F. Nathan, M. S. Rudner, N. H. Lindner, E. Berg, and G. Refael, Phys. Rev. Lett. **119**, 186801 (2017).
- <sup>30</sup> P. Titum, E. Berg, M. S. Rudner, G. Refael, and N. H. Lindner, Phys. Rev. X **6**, 021013 (2016).
- <sup>31</sup> A. Quelle, C. Weitenberg, K. Sengstock, and C. Morais Smith, New J. Phys. **19**, 113010 (2017).
- <sup>32</sup> F. Harper and R. Roy, Phys. Rev. Lett. **118**, 115301 (2017).
- <sup>33</sup> M. H. Kolodrubetz, F. Nathan, S. Gazit, T. Morimoto, and J. E. Moore, Phys. Rev. Lett. **120**, 150601 (2018), 1711.00014.
- <sup>34</sup> X. Liu, F. Harper, and R. Roy, Phys. Rev. B **98**, 165116 (2018).
- <sup>35</sup> A. Lazarides, A. Das, and R. Moessner, Phys. Rev. Lett. **115**, 030402 (2015).
- <sup>36</sup> P. Ponte, Z. Papić, F. Huveneers, and D. A. Abanin, Phys. Rev. Lett. **114**, 140401 (2015).
- <sup>37</sup> D. A. Abanin, W. D. Roeck, and F. Huveneers, Annals of Physics **372**, 1 (2016).
- <sup>38</sup> F. Nathan, D. Abanin, E. Berg, N. H. Lindner, and M. S. Rudner, arXiv:1712.02789 (2017).
- <sup>39</sup> R. Nandkishore and S. Gopalakrishnan, Annalen der Physik **529**, 1600181 (2016).
- <sup>40</sup> M. Serbyn, Z. Papić, and D. A. Abanin, Physical Review Letters **111** (2013).
- <sup>41</sup> D. A. Huse, R. Nandkishore, and V. Oganesyan, Phys. Rev. B **90**, 174202 (2014).
- <sup>42</sup> D. A. Abanin, E. Altman, I. Bloch, and M. Serbyn, arXiv:1804.11065 (2018).
- <sup>43</sup> The time-averaged current  $\bar{I}_C$  is obtained by transforming the time-dependent operator  $I_C(t)$  with the time-dependent unitary transformation  $U(t)$  in the integral above.
- <sup>44</sup> This follows from straightforward generalization of the arguments in Ref. 50 to periodically driven systems.
- <sup>45</sup> Note that Ampere's law is only meaningful when the current density has zero divergence. The long-time-averaged magnetization density  $\bar{m}_p$  in an MBL system is always well-defined, since the time-averaged current density always has zero divergence. Moreover, while Ampere's law only defines magnetization density up to a constant shift,  $\bar{m}_p$  is uniquely defined by the definition in Sec. II.A.
- <sup>46</sup> Specifically, this choice of Peierls' phases ensures that the net phase gained by traversing a closed curve is given by  $\phi_{pq}$  if the curve encircles only plaquette  $p$  (in the counterclockwise direction), and by  $-\phi_{pq}$  if the curve only encircles plaquette  $q$  (counterclockwise). The net phase is given by 0 if the curve encircles both or neither of the plaquettes.
- <sup>47</sup> For a finite system, the fact that  $m_{\alpha_1 \dots \alpha_k}^p$  is exponentially insensitive to the details of the system far away from the plaquette  $p$  means that it may only change by an amount of order  $e^{-L/\xi}$  when the system size is increased. This implies that the sum  $\sum_{\alpha_1 \dots \alpha_k} m_{\alpha_1 \dots \alpha_k}^p$  is given by its value in the thermodynamic limit, up to a correction of order  $e^{-L/\xi}$ .
- <sup>48</sup> For noninteracting systems,  $\bar{m}_p$  is a one-body operator, and  $m_{\alpha_1 \dots \alpha_k}^p = 0$  when  $k \geq 2$ . Hence only  $\mu_1$  may be nonzero [see Eq. (13)]. In this case, Eq. (12) implies that  $\text{Tr}_k \bar{m}_p = \binom{D-1}{k-1} \mu_1$ . Using  $D = L^2$ , we see that  $\binom{D-1}{k-1}$  scales as  $L^{2(k-1)}$  with the system size  $L$ .
- <sup>49</sup> In case of degeneracies, one can always pick a basis of eigenstates where  $\bar{m}_p$  is diagonal.
- <sup>50</sup> A. Chandran, I. H. Kim, G. Vidal, and D. A. Abanin, Physical Review B **91** (2015).
- <sup>51</sup> To see this, note that  $\hat{n}_\alpha |\Psi_{\mathcal{R}}\rangle = (1 - f_\alpha f_\alpha^\dagger) |\Psi_{\mathcal{R}}\rangle$ . The operator  $f_\alpha^\dagger$  is a polynomial in  $\{c_\alpha\}$  and  $\{c_\alpha^\dagger\}$ , where each term has the net effect of creating one fermion in the region around LIOM  $a$ . Since all sites near the LIOM  $a$  are occupied for the state  $|\Psi_{\mathcal{R}}\rangle$ ,  $f_\alpha^\dagger |\Psi_{\mathcal{R}}\rangle = 0$ , and thus  $\hat{n}_\alpha |\Psi_{\mathcal{R}}\rangle = |\Psi_{\mathcal{R}}\rangle$ .
- <sup>52</sup> To see that the sum in Eq. (28) converges, note that the coefficient  $m_{\alpha_1 \dots \alpha_\ell}^p$  is exponentially suppressed in  $d/\xi$ , where  $d$  is the distance from any of the LIOM centers  $\mathbf{r}_{\alpha_1} \dots \mathbf{r}_{\alpha_\ell}$  to the plaquette  $p$ . The number of distinct LIOMs whose centers are located within a radius  $\xi$  from the plaquette  $p$  is of order  $\xi^2/a^2$ , where  $a$  is the lattice constant in the system. Therefore, the coefficient  $m_{\alpha_1 \dots \alpha_\ell}^p$  vanishes exponentially when  $\ell \gg \xi^2/a^2$ . Recalling that  $\mu_\ell \equiv \sum_{\alpha_1 \dots \alpha_\ell} m_{\alpha_1 \dots \alpha_\ell}^p$  must take integer value for each  $\ell$ , we thus conclude that  $\mu_\ell$  equals zero when  $\ell \gg \xi^2/a^2$ .
- <sup>53</sup> When restricted to the subspace with  $\ell$  particles or less, the Floquet operator can be represented in terms of LIOMs  $\{\hat{n}_{\alpha_1 \dots \alpha_\ell}\}$  as in Eq. (1). Here the LIOM operators  $\{\hat{n}_{\alpha_1 \dots \alpha_\ell}\}$  have all of the properties described in Sec. I when restricted to the subspace with  $\ell$  particles or less.
- <sup>54</sup> The boundedness of bond currents in the system puts an

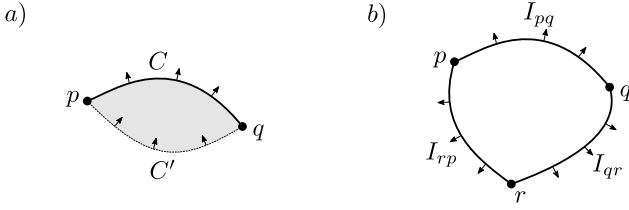


FIG. 5. a) Schematic depiction of the argument showing that time-averaged current through a cut  $C$  between two plaquettes  $p$  and  $q$  only depends on the cut's two end-points. Specifically, since there can be no accumulation of charge over time in the region between the cuts  $C$  and  $C'$ , the same current must pass through the two cuts, and thus  $\bar{I}_C = \bar{I}_{C'}$  for any two cuts  $C$  and  $C'$  between the plaquettes  $p$  and  $q$ . b) The vanishing divergence of current implies that  $\bar{I}_{C_{pq}} + \bar{I}_{C_{qr}} = \bar{I}_{C_{pr}}$ .

upper bound on  $|\langle \bar{M} \rangle|$  for any state. Hence the distribution of  $\langle \bar{M} \rangle$  must have a finite variance  $\sigma^2$  and  $M_0$  is not dominated by “rare” initial states. The mean value of  $\langle \bar{M} \rangle$  for a finite number of initial states,  $\mathcal{N}$ , is therefore given by  $M_0 + \mathcal{O}(\sigma/\sqrt{\mathcal{N}})$  for  $\mathcal{N} \gg 1$ .

- <sup>55</sup> D. Gross, V. Nesme, H. Vogts, and R. F. Werner, *Communications in Mathematical Physics* **310**, 419 (2012).
- <sup>56</sup> H. C. Po, L. Fidkowski, A. Vishwanath, and A. C. Potter, *Physical Review B* **96**, 245116 (2017).
- <sup>57</sup> The fact that the total flux on the torus is given by an integer multiple of  $2\pi$  means that this requirement does not require a specification of the interior region of the loop.
- <sup>58</sup> Here  $\|M\|$  refers to the maximum singular value norm  $\|M\| \equiv \max_{|\psi\rangle} \sqrt{\langle \psi | M^\dagger M | \psi \rangle} / \langle \psi | \psi \rangle$ .
- <sup>59</sup> This can be verified using  $\|U|\Psi\rangle\| = \|\Psi\|$  for any unitary operator  $U$ .
- <sup>60</sup> We assume that MBL is robust to perturbations, and thus  $\tilde{U}$  also describes a many-body localized system.
- <sup>61</sup> M. L. Mehta, *Random Matrices*. (Elsevier, Amsterdam, 2004).
- <sup>62</sup> Here the tensor product  $|\psi_1\rangle_A \otimes |\psi_2\rangle_B$  is defined as  $\hat{C}_1^\dagger \hat{C}_2^\dagger |0\rangle$ , where  $\hat{C}_1^\dagger$  is the unique combination of fermionic creation operators that creates the state  $|\psi_1\rangle_A$ , i.e.,  $|\psi_1\rangle_A = \hat{C}_1^\dagger |0\rangle_A$ , where  $|0\rangle_A$  denotes the vacuum in subsystem  $A$ .  $\hat{C}_2^\dagger$  is defined in a similar fashion.

## Appendix A: Proof of Eq. (5)

In this appendix we establish that the time-averaged current that passes through a cut  $C$  between two plaquettes  $p$  and  $q$  is determined by two quasilocal operators,  $\bar{m}_p$  and  $\bar{m}_q$ , with support centered at  $p$  and  $q$ , respectively [see Eq. (5) and Fig. 5]. By considering two plaquettes separated by a distance much longer than the localization length, this provides a prescription for uniquely identifying the magnetization density operator  $\bar{m}_p$  (up to exponentially small corrections in the distance, which can be of order the system size).

The operator  $I_C(t)$  that counts the current through

the cut  $C$  is given by

$$I_C(t) = \sum_{b \in B_C} I_b(t), \quad (\text{A1})$$

where  $I_b$  denotes the bond current operator on bond  $b$ , and the sum runs over all bonds that cross the cut  $C$ . Note that  $I_b(t)$ , and thereby  $I_C(t)$ , which are written in the Schrödinger picture, depend on time due to the explicit time-dependence of the Hamiltonian  $H(t)$ . In the following, we are interested in finding the time-averaged expectation value of the current,  $\langle\langle I_C \rangle\rangle$ , resulting from some given initial state  $|\psi\rangle$ . As in the main text, we use  $\langle\langle \mathcal{O} \rangle\rangle \equiv \lim_{\tau \rightarrow \infty} \frac{1}{\tau} \int_0^\tau dt \langle \psi(t) | \mathcal{O}(t) | \psi(t) \rangle$ .

The time-averaged expectation value of the current  $I_C$  may equivalently be computed in the Heisenberg picture as  $\langle\langle I_C \rangle\rangle = \langle \psi | \bar{I}_C | \psi \rangle$ , where  $|\psi\rangle$  denotes the initial state of the system, and  $\bar{I}_C$  denotes the time-average of the current  $I_C$  in the Heisenberg picture. Specifically, for any Schrödinger picture operator  $\mathcal{O}(t)$ ,  $\bar{\mathcal{O}}$  is defined as

$$\bar{\mathcal{O}} \equiv \lim_{\tau \rightarrow \infty} \frac{1}{\tau} \int_0^\tau dt U^\dagger(t) \mathcal{O}(t) U(t). \quad (\text{A2})$$

The time-averaged current operator  $\bar{I}_C$  is thus obtained by transforming the time-dependent operator  $I_C(t)$  in Eq. (A1) with evolution operator  $U(t)$ , and integrating over time as in Eq. (A2).

To explore the properties of the time-averaged current operator  $\bar{I}_C$ , we consider the time-averaged current for a different cut,  $C'$ , between the same two plaquettes  $p$  and  $q$ , see Fig. 2a. We note that  $I_C(t) - I_{C'}(t) = \dot{N}_R(t)$ , where  $N_R$  measures the number of particles in the region  $R$  between cut  $C$  and  $C'$  (shaded region). Importantly, since  $N_R$  is bounded by the number of sites in the region  $R$ , the long-time-averaged value of  $\langle \dot{N}_R \rangle$  must vanish. We thus conclude that  $\langle\langle I_C \rangle\rangle = \langle\langle I_{C'} \rangle\rangle$ . Since this result holds for any initial state  $|\psi\rangle$ , we conclude that

$$\bar{I}_C = \bar{I}_{C'}. \quad (\text{A3})$$

As a next step, we note from Eq. (A1) that  $\bar{I}_C = \sum_{b \in B_C} \bar{I}_b$ , where  $\bar{I}_b$  denotes the time-averaged current on bond  $b$  [see Eq. (A2)]. We note that the operator  $I_b(t)$  is local, with support only on the sites connected by the bond  $b$ . For many-body localized systems, this implies that the operator  $\bar{I}_b$  is a localized integral of motion, with support within a distance  $\sim \xi_l$  from the bond  $b$ , up to an exponentially small correction<sup>44</sup>. Hence,  $\bar{I}_C$  is given by a sum of terms, each of which only has support within a region of radius  $\xi_l$ , centered at a point along the cut  $C$ .

The requirements that  $\bar{I}_C$  is given by a sum of local terms as described above, while at the same time taking the same value for all cuts between plaquettes  $p$  and  $q$  [Eq. (A3)], significantly constrains the form that  $\bar{I}_C$  can take. In particular, this implies that  $\bar{I}_C = I(p, q)$ , where the operator  $I(p, q)$  only depends on the locations of the two plaquettes  $p$  and  $q$  (and not on the details of the cut

C). Moreover, for any cut between plaquettes  $p$  and  $q$ ,  $I(p, q)$  is given by a sum of terms which only have support in a region of width  $\xi_l$  around the cut. For any site located a distance larger than  $\xi_l$  from both plaquettes  $p$  or  $q$ , we can find a cut that remains separated from the site by a distance larger than  $\xi_l$ . Therefore the support of operator  $I(p, q)$  can only include sites within a localization length of the endpoints  $p$  and  $q$ . Hence, we write:

$$I(p, q) = A_1(p, q) + A_2(p, q), \quad (\text{A4})$$

where  $A_1(p, q)$  has its full support within a region of width  $\xi_l$  around plaquette  $p$ , and  $A_2(p, q)$  has support around plaquette  $q$ . The operators  $A_1(p, q)$  and  $A_2(p, q)$  depend only on the locations of plaquettes  $p$  and  $q$ , respectively.

By letting the cut from  $p$  to  $q$  go through an arbitrary plaquette  $r$  on the torus (see Fig. 2b), we conclude from the arguments above the  $I(p, r) + I(r, q) = I(p, q)$ . This implies

$$A_1(p, r) + A_2(p, r) + A_1(r, q) + A_2(r, q) = A_1(p, q) + A_2(p, q). \quad (\text{A5})$$

The only terms on the left hand side with support near plaquette  $r$  are the terms  $A_2(p, r)$ , and  $A_2(r, q)$ , while none of the terms on the right-hand side have support near plaquette  $r$ . We thus conclude that  $A_2(p, r) = -A_1(r, q)$  for any choice of two plaquettes  $p$  and  $q$ . Hence we may write  $A_1(r, q) = A(r)$ , and  $A_2(p, r) = -A(r)$  for some function  $A(r)$  which only depends on the location of plaquette  $r$  and has its full support near plaquette  $r$ . Using this in Eq. (A4), we find

$$I(p, q) = A(p) - A(q). \quad (\text{A6})$$

Identifying  $A(p) = \bar{m}_p$ , we thus conclude that Eq. (5) holds.

## Appendix B: Response of system to the insertion of a magnetic flux

Here we provide technical details of the discussion in Sec. II.D of the main text, where the integer quantization of the invariants  $\{\mu_\ell\}$  is discussed. Specifically, we establish here the relation between the magnetization coefficient  $m_{\alpha_1 \dots \alpha_\ell}^p$  and the response of the corresponding quasienergy coefficient to the insertion of a uniform magnetic field  $B_0 = 2\pi/L^2$  [Eq. (22) in the main text]:

$$\frac{\tilde{\varepsilon}_{\alpha_1 \dots \alpha_\ell} - \varepsilon_{\alpha_1 \dots \alpha_\ell}}{B_0} = a^2 \sum_p m_{\alpha_1 \dots \alpha_\ell}^p, \quad (\text{B1})$$

where  $\tilde{\varepsilon}_{\alpha_1 \dots \alpha_\ell}$  denotes the ‘‘perturbed’’ quasienergy coefficient of the one-flux system corresponding to the unperturbed quasienergy coefficient  $\varepsilon_{\alpha_1 \dots \alpha_\ell}$  (see Sec. II.D).

Note that Eq. (22) does not follow trivially from first-order perturbation theory in the field  $B_0$ : under

a continuous perturbation of the system, the system’s quasienergy spectrum undergoes exponentially many avoided crossings due to resonances between Floquet eigenstates separated by a large distance in Fock space. Hence, first-order perturbation theory breaks down for the system. Instead, we establish Eq. (22) with an alternative approach, using the localization properties of the  $k$ -particle Floquet eigenstates  $\{|\Psi_{\alpha_1 \dots \alpha_k}\rangle\}$ .

In order to follow this approach, we use a succession of auxiliary results which are not discussed in detail in the main text, but are crucial for the proof of Eq. (22). The line of arguments proceeds as follows: we first show explicitly how the uniform magnetic field  $B_0$  can be implemented in the system (Sec. B.1). Subsequently, we show that, for any finite (simply connected) region  $R$  of the lattice, it is always possible to choose a gauge where the Hamiltonian  $\tilde{H}$  of the one-flux system resembles the Hamiltonian  $H$  of the zero-flux system locally within  $R$  (Sec. B.2), and likewise for the Floquet operators  $\tilde{U}$  and  $U$  (Sec. B.3). From this, we demonstrate that the  $k$ -particle Floquet eigenstates and quasienergies of a many-body localized system are robust to perturbations, including the insertion of the weak uniform magnetic field  $B_0$  (Sec. B.4). Finally, using this result, we prove Eq. (22) (Sec. B.5), which is the goal of this appendix.

### 1. Implementation of magnetic flux

Here we briefly discuss how the magnetic flux is implemented. The system we consider consists of interacting fermions on a lattice with the geometry of a torus, of dimensions  $L \times L$ . The Hamiltonian of the system (in the absence of a flux) takes the form

$$H(t) = \sum_{ij} J_{ij}(t) \hat{c}_i^\dagger \hat{c}_j + H_{\text{int}}(t), \quad (\text{B2})$$

where  $c_i$  annihilates a fermion on site  $i$  in the lattice. Here the first term contains both hopping and on-site potentials, including disorder, with  $J_{ij}(t) = J_{ji}^*(t)$ , while the term  $H_{\text{int}}$  accounts for interactions. We allow both parts of the Hamiltonian to be time-dependent, with periodicity  $T$ . To simplify the discussion, we consider the case of a square lattice model with nearest-neighbour hoppings, and a density-density interaction described by  $H_{\text{int}} = \frac{1}{2} \sum_{i,j} \rho_i \rho_j V_{ij}$ , where  $\rho_i = \hat{c}_i^\dagger \hat{c}_i$  and  $V_{ij} = V_{ji}$  is real. In the general case of a quasilocal Hamiltonian, the results below can also be derived using similar arguments.

In this subsection we are interested in finding the Hamiltonian  $\tilde{H}$  of the system when the uniform magnetic field  $B_0 = \frac{2\pi}{L^2}$  is inserted, corresponding to one flux quantum through the surface of torus. Having assumed  $H_{\text{int}}$  to consist of density-density interactions, only the first term in Eq. (B2) is affected by the magnetic flux. The Hamiltonian  $\tilde{H}$  thus takes the form:

$$\tilde{H} = \sum_{ij} e^{-i\theta_{ij}} J_{ij}(t) \hat{c}_i^\dagger \hat{c}_j + H_{\text{int}}(t). \quad (\text{B3})$$

Here, the Peierls phases  $\{\theta_{ij}\}$ , with  $\theta_{ij} = -\theta_{ji}$ , must ensure that the total phase acquired by traversing a closed loop on the torus is given by  $B_0 A_S \pmod{2\pi}$ , where  $A_S$  is the area enclosed by the loop<sup>57</sup>. There are (infinitely) many distinct configurations of the phases  $\{\theta_{ij}\}$  that satisfy this condition, corresponding to different choices of gauge for the one-flux Hamiltonian  $\tilde{H}$ .

The goal of the following is to show that we can choose a gauge where the flux  $B_0$  only weakly perturbs the Hamiltonian within a particular finite disk-shaped region  $R$  of the lattice. To do this, we seek a gauge where the Peierls phases  $\theta_{ij}$  are all much smaller than 1 for bonds located within  $R$ . We take region  $R$  to have area  $A_R \ll L^2$ , and to be centered around the location  $\mathbf{r}_0 = (x_0, y_0)$  on the torus. We assume furthermore for simplicity that  $\mathbf{r}_0$  is far away from either of the branch cuts of the position operator at  $x = L$  and/or  $y = L$ .

To keep the Peierls phases small within  $R$ , we employ the following Landau-type gauge. Let  $\theta_i^x$  denote the Peierls phase for hopping along the bond in the positive  $x$ -direction from site  $i$  (and similarly let  $\theta_i^y$  be the Peierls phase for hopping in the positive  $y$ -direction), and give them the values:

$$\theta_i^y = B_0(x_i - x_0)a \quad \theta_i^x = B_0 L y_i \delta_{x_i, L}. \quad (\text{B4})$$

Here  $x_i$  and  $y_i$  denote the coordinates of site  $i$ , and  $\delta_{ij}$  denotes the Kronecker delta symbol, such that  $\delta_{x_i, L}$  takes value 1 if  $x_i = L$ , while  $\delta_{x_i, L} = 0$  for all other values of  $x_i$ . Recall that  $a$  is the lattice constant. The phases  $\theta_i^y$  ensure that a trajectory encircling a plaquette acquires a phase of  $B_0 a^2$ , if the trajectory does not cross the branch cut of the  $x$ -position operator between  $x = L$  and  $x = 0$ . The phase  $\theta_i^x$ , which does not appear in the Landau gauge in an open geometry, is necessary to ensure that the phase is also given by  $B_0 a^2 \pmod{2\pi}$  for trajectories encircling plaquettes across the branch cut.

To see that the gauge choice in Eq. (B4) implies that the Peierls phases are much smaller than 1 in the region  $R$ , note that  $\mathbf{r}_0$  is located far from the branch cut at  $x = 0, L$ . Hence  $\theta_i^x = 0$  for all sites in the region  $R$ . To see that  $\theta_i^y$  is much smaller than 1, note that  $|x_i - x_0| \leq \sqrt{A_R}$  when the site  $i$  is located within  $R$ . This follows from the fact that  $R$  has disk geometry, and is centered around  $\mathbf{r}_0$ . Thus  $\theta_i^y$  is maximally of order  $\sqrt{A_R}a/L^2$  for sites within  $R$ , and therefore much smaller than 1 in the limit  $A_R \ll L^2$  specified above.

## 2. Response of the Hamiltonian

An important result we will use extensively in the following is that, for large systems, the insertion of the uniform field  $B_0$  only weakly perturbs the system, up to a gauge transformation. To see this, we consider the action of  $\tilde{H} - H$  on a state  $|\psi\rangle$  where all particles are located in the finite region  $R$  that was introduced in the previous subsection.

As a first step, we note that  $(\tilde{H} - H)|\psi\rangle = (\tilde{H} - H)P_R|\psi\rangle$ , where  $P_R$  projects into the subspace where all particles are confined to  $R$ . Using that  $\hat{c}_i P_R = 0$  if site  $i$  is located outside  $R$ , we find

$$[\tilde{H}(t) - H(t)]P_R = \sum_{j \in R} \sum_i J_{ij}(t) \hat{c}_i^\dagger \hat{c}_j (e^{-i\theta_{ij}} - 1). \quad (\text{B5})$$

The Peierls phases  $\{\theta_{ij}\}$  are as given in Eq. (B4) above. Below, we show that the operator  $(\tilde{H} - H)P_R$  is small when the system size is large. Specifically, we will find an upper bound for the norm<sup>58</sup>  $\|(\tilde{H} - H)P_R\|$ . In order to do this, we make use of the fact that  $\|M\| \leq \sqrt{\text{Tr}(M^\dagger M)}$ , such that

$$\|(\tilde{H} - H_0)P_R\|^2 \leq \sum_{j_1, j_2 \in R} \sum_{i_1, i_2} K_{i_1 j_1}^* K_{i_2 j_2} \text{Tr}(\hat{c}_{j_1}^\dagger \hat{c}_{i_1} \hat{c}_{i_2}^\dagger \hat{c}_{j_2}),$$

where  $K_{ij} \equiv J_{ij}(e^{i\theta_{ij}} - 1)$ . Noting that  $\theta_{ij} = 0$  for  $i = j$ , we see that the terms above are only non-vanishing when  $i_1 = i_2$  and  $j_1 = j_2$ . Thus, we find

$$\|(\tilde{H} - H_0)P_R\|^2 \leq \sum_{j \in R} \sum_i |J_{ij}|^2 |e^{-i\theta_{ij}} - 1|^2. \quad (\text{B6})$$

We now estimate the maximal scale of the right hand side above. We recall from the discussion in the end of Subsection B.1 that the Peierls phases  $\{\theta_{ij}\}$ , as given in Eq. (B4), are of order  $\sqrt{A_R}a/L^2$  or smaller for bonds within the region  $R$ . This implies that the value of each non-vanishing term in the sum in Eq. (B6) is of order  $J^2 A_R a^2 / L^4$  or less, where  $J$  denotes the typical scale of the (off-diagonal) tunnelling coefficients  $\{J_{ij}\}$ . To estimate the number of non-vanishing terms in the sum we recall, from the assumptions made in the beginning of subsection B.1, that the tunneling coefficients  $J_{ij}$  only couple nearest-neighbor pairs of sites in the lattice. Hence, for each choice of the index  $j$ ,  $J_{ij}$  may only be non-vanishing for four choices of the index  $i$ . These considerations show that there are only of order  $A_R/a^2$  non-vanishing terms in the sum above. Using that each non-vanishing term is of order  $J^2 A_R a^2 / L^4$  or less, we find that  $\|(\tilde{H} - H)P_R\|^2 \lesssim A_R^2 J^2 L^{-4}$ . Here  $a \lesssim b$  indicates that  $a$  is smaller than  $b$ , or of order  $b$ . Thus we conclude that

$$\|(\tilde{H} - H)P_R\| \lesssim J A_R / L^2. \quad (\text{B7})$$

In the sense of the operator norm, the difference between the Hamiltonians with and without one flux quantum uniformly piercing the entire torus decays to zero with the inverse of the total system area, when acting on states confined to any given disk-shaped region  $R$ , and with a judicious choice of gauge.

### a. Action on a localized state

Using the above result, we now show that it is possible to choose a gauge such that  $(H - \tilde{H})$  is small when



acting on a state which is not strictly confined to the disk-shaped region  $R$  of the lattice, but rather only exponentially localized. Specifically, we consider a state  $|\psi\rangle$ , whose full support is confined to a disk-shaped region  $R$  of physical radius  $r$ , with probability of finding a particle a distance  $s$  from the center of  $R$  decaying as  $e^{-s/\xi_l}$  when  $s > r$ .

We first write  $|\psi\rangle = \sum_j |\psi_j\rangle$ , where  $|\psi_j\rangle = (P_j - P_{j-1})|\psi\rangle$ , and  $P_j$  is a projector onto the states where *all* particles are located within a distance  $ja$  from the center of  $R$ . Note that  $P_j P_k = P_{\min(j,k)}$ . Using this relation, one can verify by direct computation that the states  $\{|\psi_j\rangle\}$  are orthogonal:  $\langle\psi_j|\psi_k\rangle = 0$  if  $j \neq k$ . We furthermore note that the norm of the state  $|\psi_j\rangle$  decays exponentially with  $j$  for  $ja > r$ . In particular, note that  $P_j|\psi\rangle \rightarrow |\psi\rangle$  as  $j \rightarrow \infty$ . Thus  $\sum_{j=j_0+1}^{\infty} |\psi_j\rangle = (1 - P_{j_0})|\psi\rangle$  for any  $j_0$ . By computing the norm of  $(1 - P_{j_0})|\psi\rangle$ , and using that the states  $\{|\psi_j\rangle\}$  are orthogonal, one then finds

$$\langle\psi|(1 - P_{j_0})|\psi\rangle = \sum_{j>j_0} \langle\psi_j|\psi_j\rangle. \quad (\text{B8})$$

The expectation value  $\langle\psi|(1 - P_{j_0})|\psi\rangle$  gives the probability of finding a particle more than a distance  $j_0$  from the center of  $R$ ; by assumption this number is of order  $e^{-j_0 a/\xi_l}$ , when  $j_0 a > r$ . Thus, since  $\langle\psi_j|\psi_j\rangle \geq 0$ ,

$$\langle\psi_j|\psi_j\rangle \lesssim e^{-ja/\xi_l}. \quad (\text{B9})$$

when  $ja > r$ .

We now consider the state  $(\tilde{H} - H)|\psi\rangle$ . Inserting  $|\psi\rangle = \sum_j |\psi_j\rangle$ , and using  $P_j|\psi_j\rangle = |\psi_j\rangle$  one finds

$$(\tilde{H} - H)|\psi\rangle = (\tilde{H} - H)P_R|\psi\rangle + \sum_{j>r/a} (\tilde{H} - H)P_j|\psi_j\rangle.$$

Using the triangle inequality, along with Eq. (B7) and  $\| |\psi_j\rangle \| \lesssim e^{-(r+ja)/2\xi_l}$ , we obtain:

$$\|(\tilde{H} - H)|\psi\rangle\| \lesssim JA_R/L^2 + \sum_{j>r/a} \|(\tilde{H} - H)P_j\| e^{-\frac{ja}{2\xi_l}}.$$

The considerations in the previous subsection show that we may choose a gauge for  $\tilde{H}$  such that  $\|(\tilde{H} - H)P_j\| \lesssim A_{R_j}^2 J/L^2$  for any choice of  $j$ , where  $A_{R_j}$  denotes the area of the region projected into by  $P_j$ . Using  $A_{R_j} \sim (ja)^2$ , and that  $\sum_{j>j_0} j^2 e^{-j/k} \sim j_0^2 e^{-j_0/k}$  when  $j_0 \gg k$ , one can then verify that

$$\sum_{j>r/a} \|(\tilde{H} - H)P_j\| e^{-\frac{ja}{2\xi_l}} \lesssim A_R J/L^2 e^{-r/2\xi_l}, \quad (\text{B10})$$

where  $A_R \sim r^2$  denotes the area of the region  $R$ . Thus, since  $r \gg \xi_l$ , we find

$$\|(\tilde{H} - H)|\psi\rangle\| \lesssim JA_R/L^2. \quad (\text{B11})$$

### 3. Response of the Floquet operator

We now show that, for any given disk-shaped region  $R$  in the lattice, it is possible to find a gauge, the Floquet operators of the one- and zero-flux systems,  $\tilde{U}(T)$  and  $U(T)$ , have nearly identical actions states  $|\psi\rangle$  localized within  $R$ :  $\tilde{U}(T)|\psi\rangle \approx U(T)|\psi\rangle$ . Here the state is said to be localized within  $R$  if the probability of finding a particle a distance  $s$  from the center of  $R$  decays as  $e^{-s/\xi_l}$  for  $s > r$ , where  $r$  denotes the radius of  $R$ .

As a first step, we note<sup>59</sup> that  $\|(U - \tilde{U})|\psi\rangle\| = \|(\tilde{U}^\dagger U - 1)|\psi\rangle\|$ . Using the fact that  $\tilde{U}^\dagger U - 1 = \int_0^T dt \partial_t [\tilde{U}^\dagger(t)U(t)]$ , along with the chain rule, we find

$$(\tilde{U}^\dagger U - 1)|\psi\rangle = -i \int_0^T dt \tilde{U}^\dagger(t) [H(t) - \tilde{H}(t)] U(t) |\psi\rangle. \quad (\text{B12})$$

Using this result in Eq. (B12), along with the triangle inequality, gives:

$$\|(\tilde{U}^\dagger U - 1)|\psi\rangle\| \leq \int_0^T dt \| [H(t) - \tilde{H}(t)] U(t) |\psi\rangle \|, \quad (\text{B13})$$

where we used  $\|\tilde{U}^\dagger(t)|\phi\rangle\| = \|\phi\|$  for state  $|\phi\rangle$ , since  $\tilde{U}$  is unitary.

We now make use of the fact that the time-evolution operator  $U(t)$  is local at all times  $0 \leq t \leq T$ , due to the finite Lieb-Robinson velocity  $v$  of the system. The locality implies that, for the state  $U(t)|\psi\rangle$ , the probability of finding a particle a distance  $s$  from the center of  $R$  decays exponentially when  $s \gtrsim r$ . Using the result in Eq. (B11) from the previous subsection, we thus find

$$\|[\tilde{H}(t) - H(t)]U(t)|\psi\rangle\| \lesssim JA_R/L^2. \quad (\text{B14})$$

Using this in the inequality in Eq. (B13), we conclude

$$\|(U^\dagger \tilde{U} - 1)|\psi\rangle\| \lesssim JTA_R/L^2. \quad (\text{B15})$$

Thus,  $\|(\tilde{U} - U)|\psi_R\rangle\| \lesssim JTA_R/L^2$ .

The result in Eq. (B15) shows that, with a judicious choice of gauge, the Floquet operators of the one- and zero flux systems give nearly identical results when acting on a localized state. In this sense, the insertion of a uniform magnetic field  $B_0$  only weakly modifies the Floquet operator for large systems.

### 4. Response of Floquet eigenstates and quasienergy spectrum

We now use the result in Eq. (B15) to show that the quasienergy spectrum and Floquet eigenstates of the system are robust to perturbations, and only weakly affected

by the insertion of the uniform magnetic field  $B_0$ . To simplify the proof, we introduce a fixed length scale  $d \gg \xi_l$ , which acts as an effective length cutoff for the region of support of a LIOM. The length  $d$  must be much smaller than  $L$ , but can otherwise be taken to be arbitrarily large, as long as it remains finite as the thermodynamic limit is taken.

Using this cutoff length, we show below that Floquet eigenstates  $\{|\tilde{\Psi}_{\alpha_1 \dots \alpha_k}\rangle\}$  of  $\tilde{U}$  can be labeled such that, for *each* choice of LIOMs (identified by the LIOM indices  $\alpha_1 \dots \alpha_k$ ),

$$|\tilde{\Psi}_{\alpha_1 \dots \alpha_k}\rangle = |\Psi_{\alpha_1 \dots \alpha_k}\rangle + \mathcal{O}\left(e^{-d/\xi_l}\right). \quad (\text{B16})$$

Thus, *each* eigenstate of  $\tilde{U}$  is identical to an eigenstate of  $U$  (up to gauge transformation, and a vanishing correction). This is the result quoted above Eq. (22) in the main text. In addition, we show that, when the LIOMs  $\alpha_1 \dots \alpha_k$  are all located within a distance  $d$  from the same point (or  $k = 1$ )

$$\tilde{E}_{\alpha_1 \dots \alpha_k} = E_{\alpha_1 \dots \alpha_k} + \mathcal{O}\left(\frac{Jd^2}{L^2}\right). \quad (\text{B17})$$

Due to the possibility that the introduction of the field  $B_0$  induces a resonance between two Floquet eigenstates of  $U$ , disorder realizations do exist where one (or more) of the eigenstates of  $\tilde{U}$  is a significantly hybridized combination of two eigenstates of  $U$ . In this case, Eq. (B16) will hold for most but not all Floquet eigenstates of the system. However, as we show here, Eq. (B16) is only violated for a set of disorder realizations with measure zero in thermodynamic limit. In this way, Eqs. (B16) and (B17) hold for *almost all* disorder realizations, in the thermodynamic limit.

To show that Eqs. (B17) and (B16) hold, we first consider the case  $k = 1$  (i.e., we establish the relationship for each single-particle Floquet eigenstate). Subsequently, we generalize this result to larger numbers of particles.

#### a. Single-particle eigenstates

Here we establish the relationships in Eqs. (B16) and (B17) for the single-particle case. As a first step, we note that the one-flux system is also many-body localized<sup>60</sup>. Thus any (single-particle) eigenstate  $|\tilde{\Psi}\rangle$  of  $\tilde{U}$  has its full support within a finite disk-shaped region  $S$  of linear dimension  $d$ , with the probability of finding the particle a distance  $s$  outside  $S$  decaying as  $e^{-s/\xi_l}$ .

The finite region of support of  $|\tilde{\Psi}\rangle$  implies that each eigenstate  $|\tilde{\Psi}\rangle$  of  $\tilde{U}$  may only overlap significantly with a finite number  $N_1$  of eigenstates of  $U$ ; namely,  $|\tilde{\Psi}\rangle$  may only overlap with the eigenstates  $|\Psi_{\alpha_1}\rangle \dots |\Psi_{\alpha_{N_1}}\rangle$  whose corresponding LIOM centers are located within a distance  $d$  from  $S$  (up to a correction exponentially small in

$d/\xi_l$ ). Thus, we may write

$$\sum_{n=1}^{N_1} |\langle \Psi_{\alpha_n} | \tilde{\Psi} \rangle|^2 = 1 + \mathcal{O}(e^{-d/\xi_l}). \quad (\text{B18})$$

Crucially,  $N_1$  is of order  $d^2/a^2$ , and thus independent of system size. We order the indices  $n$  according to the value of the overlap, such that  $|\langle \Psi_1 | \tilde{\Psi} \rangle|^2 \geq |\langle \Psi_2 | \tilde{\Psi} \rangle|^2 \geq \dots \geq |\langle \Psi_{N_1} | \tilde{\Psi} \rangle|^2$ . Note that the sequence of LIOM indices  $\alpha_1 \dots \alpha_{N_1}$  depends on the choice of  $|\tilde{\Psi}\rangle$ ; this dependence is taken to be implicit below, for the sake of brevity.

As a next crucial step, we now show that  $|\tilde{\Psi}\rangle$  only overlaps significantly with *one* of the eigenstates  $|\Psi_{\alpha_1}\rangle \dots |\Psi_{\alpha_{N_1}}\rangle$ , while the total weight from all other eigenstates gives a negligible contribution. To show this, note that  $|\Psi_{\alpha_n}\rangle$  and  $|\tilde{\Psi}\rangle$  are eigenstates of  $U$  and  $\tilde{U}$ , respectively, and hence

$$\langle \Psi_{\alpha_n} | \tilde{\Psi} \rangle = \frac{\langle \Psi_{\alpha_n} | U^\dagger \tilde{U} - 1 | \tilde{\Psi} \rangle}{e^{-i(\tilde{E} - E_{\alpha_n})T} - 1}, \quad (\text{B19})$$

where  $\tilde{E}$  is the quasienergy associated with  $|\tilde{\Psi}\rangle$ . We now make use of the results from the previous subsection [Sec. B.3]: since  $|\tilde{\Psi}\rangle$  is exponentially well localized within the region  $S$ , the inequality (B15) implies that  $|\langle \Psi_{\alpha_n} | U^\dagger \tilde{U} - 1 | \tilde{\Psi} \rangle| \lesssim JTA_S/L^2$ . We also note that  $|e^{-i(\tilde{E} - E_{\alpha_n})T} - 1| \leq |\tilde{E} - E_n|$ , where the norm  $|\cdot|$  is defined modulo  $2\pi/T$ , i.e.  $|E| \equiv \min_z |E + 2\pi z/T|$ . Using these two inequalities in Eq. (B19), we conclude

$$|\langle \Psi_{\alpha_n} | \tilde{\Psi} \rangle| \lesssim \frac{JA_S/L^2}{|\tilde{E} - E_{\alpha_n}|}. \quad (\text{B20})$$

We now consider two implications of the above inequality. Firstly, since Eq. (B18) implies that  $|\langle \Psi_{\alpha_1} | \tilde{\Psi} \rangle|^2 \gtrsim 1/N_1 - \mathcal{O}(e^{-d/\xi_l})$  (c.f. the labelling of the states  $\{|\Psi_n\rangle\}$ ), we must have

$$|\tilde{E} - E_{\alpha_1}| \lesssim \frac{\sqrt{N_1}JA_R}{L^2}. \quad (\text{B21})$$

Secondly, we note that, for a random choice of  $|\tilde{\Psi}\rangle$ , the typical spacing between the  $N_1$  quasienergy levels  $\{E_n\}$  is of order  $\Delta E \sim \mathcal{W}/N_1$ , where  $\mathcal{W}$  denotes the width of the single-particle quasienergy spectrum (when the quasienergy spectrum has no gaps,  $\mathcal{W} = 2\pi/T$ ). In this case, only one of the quasienergies  $\{E_n\}$  (namely  $n = 1$ ) is therefore close enough to  $\tilde{E}$  for Eq. (B20) to allow a significant value of  $\langle \Psi_n | \tilde{\Psi} \rangle$ . Thus,  $|\tilde{\Psi}\rangle \approx |\Psi_1\rangle$  for a typical choice of  $|\tilde{\Psi}\rangle$ .

We now prove that  $|\tilde{\Psi}\rangle \approx |\Psi_1\rangle$  for *any* choice of  $|\tilde{\Psi}\rangle$  in the system (except for a measure-zero set of disorder realizations in the thermodynamic limit). To establish this result, we first note

$$|E_n - \tilde{E}| \geq |E_n - E_{\alpha_1}| - |\tilde{E} - E_{\alpha_1}|. \quad (\text{B22})$$

We now establish a lower bound for  $|E_{\alpha_1} - E_{\alpha_n}|$ , using the fact the quasienergy levels of nearby states  $E_{\alpha_1}$  and  $E_{\alpha_n}$  repel each other, and that  $|E_{\alpha_1} - \tilde{E}|$  is bounded. Specifically, note that the Floquet eigenstates  $|\Psi_1\rangle$  and  $|\Psi_n\rangle$  have their support within a distance  $\lesssim d$  from each other. The quasienergies  $E_1$  and  $E_n$  are hence subject to local level repulsion when the quasienergy difference  $\delta E \equiv |E_n - E_1|$  is much smaller than the scale of matrix elements between them with respect to the kinetic part of the Hamiltonian (i.e.  $\delta E \ll J e^{-d/\xi_t}$ ). In the limit where  $\delta E \ll J e^{-d/\xi_t}$ , the probability distribution  $p(\delta E)$  for  $\delta E$  should thus resemble the Wigner-Dyson distribution for the Circular unitary ensemble (CUE)<sup>61</sup>:

$$p(\delta E) = \frac{T^3}{\pi} \delta E^2 + \mathcal{O}(\delta E^4). \quad (\text{B23})$$

Using the above result, we now compute the expected number of pairs of nearby single-particle eigenstates  $|\Psi_{\alpha_i}\rangle$  and  $|\Psi_{\alpha_j}\rangle$  in the entire system, for which  $|E_{\alpha_i} - E_{\alpha_j}|$  is smaller than some given (small) value  $\delta E_0$  (note that the eigenstates and quasienergies are labelled with respect to the labelling scheme prescribed in the main text). Here “nearby” refers to the eigenstates  $|\Psi_{\alpha_i}\rangle$  and  $|\Psi_{\alpha_j}\rangle$  having their centers located within a distance  $\sim d$  from each other, such that they may potentially overlap with the same eigenstate of  $\tilde{U}$ . Noting that there are  $\mathcal{O}(L^2 N_1 / 2a^2)$  distinct pairs of nearby eigenstates, we have

$$N(\delta E_0) = \frac{L^2 N_1}{2a^2} \int_0^{\delta E_0} d\delta E p(\delta E). \quad (\text{B24})$$

Thus, in the limit where  $\delta E_0 \ll J e^{-d/\xi_t}$ ,

$$N(\delta E_0) = \frac{L^2 N_1 (\delta E_0 T)^3}{6\pi a^2}. \quad (\text{B25})$$

The above result in particular implies that  $N(\frac{a}{LT}) = 0$  in the thermodynamic limit. Hence, in the thermodynamic limit, there are zero pairs of nearby eigenstates  $|\Psi_{\alpha_i}\rangle$  and  $|\Psi_{\alpha_j}\rangle$  whose quasienergy differs by less than  $\frac{a}{LT}$ , except for in a measure zero set of disorder realizations. We conclude, in the thermodynamic limit, and for any choice of  $|\tilde{\Psi}\rangle$ ,

$$|E_{\alpha_1} - E_{\alpha_n}| > \frac{a}{LT} \quad (\text{B26})$$

for all but a measure zero set of disorder realizations.

Using the triangle inequality [Eq. (B22)], and the fact that that  $|\tilde{E} - E_{\alpha_1}|$  is subleading in  $L$  compared to the above bound for  $|E_{\alpha_n} - E_{\alpha_1}|$ , we have, for  $n \geq 2$ ,  $|\tilde{E} - E_{\alpha_n}| > \frac{a}{LT}$ . Thus, for  $n \geq 2$ , it holds, for *each* choice of  $|\tilde{\Psi}\rangle$  that

$$|\langle \Psi_{\alpha_n} | \tilde{\Psi} \rangle| < \frac{A_R J T a}{L}, \quad (\text{B27})$$

except for a measure zero set of disorder realizations. Using this result in Eq. (B18), we find

$$1 - |\langle \Psi_{\alpha_1} | \tilde{\Psi} \rangle|^2 < \frac{N_1 A_R^2 J^2 T^2 a^2}{L^2} + \mathcal{O}(e^{-d/\xi_t}). \quad (\text{B28})$$

In the thermodynamic limit  $L \rightarrow \infty$ , where  $d$  remains fixed, the correction term dominates on the right hand side, and we find

$$|\langle \Psi_{\alpha_1} | \tilde{\Psi} \rangle|^2 = 1 - \mathcal{O}(e^{-d/\xi_t}). \quad (\text{B29})$$

Recall that the effective cutoff  $d$  can be picked arbitrarily large, as long as it remains finite. This concludes the proof of Eq. (B16) for the single-particle case, when we assign the label  $\alpha_1$  to  $|\tilde{\Psi}\rangle$ .

To prove that Eq. (B17) holds, we note from Eq. (B20) [with the labelling introduced below Eq. (B16)] that, for each choice of  $\alpha$ ,

$$|\tilde{E}_\alpha - E_\alpha| \lesssim \frac{J A_R / L^2}{|\langle \tilde{\Psi}_\alpha | \Psi_\alpha \rangle|}. \quad (\text{B30})$$

Since  $|\langle \tilde{\Psi}_\alpha | \Psi_\alpha \rangle| \approx 1$ , and  $A_S \sim d^2$ , we conclude  $|\tilde{E}_\alpha - E_\alpha| \lesssim J d^2 / L^2$ . This is what we wanted to show.

### b. Two-particle eigenstates

Having established the relationship in Eq. (B16) for single-particle Floquet eigenstates, we now show that it also holds for all two-particle eigenstates. In order to do this, we consider a two-particle Floquet eigenstate  $|\tilde{\Psi}\rangle$  of the one-flux system, with quasienergy  $\tilde{E}$ . Since the one-flux system is many-body localized, the eigenstates of  $\tilde{U}$  possess a LIOM structure. In the Floquet eigenstate  $|\tilde{\Psi}\rangle$ , two of the LIOMs of  $\tilde{U}$   $\tilde{n}_1$  and  $\tilde{n}_2$  are “excited” (i.e. have nonzero expectation value). In the following, we divide our argumentation into two cases, depending on whether or not the two LIOMs are located within a distance  $d$  from each other, where the arbitrarily large (but fixed) length was introduced in the beginning of Sec. B.4.a.

*Nearby LIOMs* — We first consider the case where the centers of the two “excited” LIOMs  $\tilde{n}_1$  and  $\tilde{n}_2$  in the state  $|\tilde{\Psi}\rangle$  are separated by a distance less than  $d$ . In this case, for a two-particle Floquet eigenstate  $|\Psi_{\alpha\beta}\rangle$  of the one-flux system to significantly overlap with  $|\tilde{\Psi}\rangle$ , the LIOMs  $\hat{n}_\alpha$  and  $\hat{n}_\beta$  must be located within a distance  $d$  from the centers of  $\tilde{n}_1$  and  $\tilde{n}_2$ . This implies that there are only of order  $N_2 \sim \binom{2d^2/a^2}{2}$  choices of distinct LIOMs  $\alpha, \beta$  for which  $|\Psi_{\alpha\beta}\rangle$  significantly overlaps with  $|\tilde{\Psi}\rangle$ .

Using the same arguments as for the single particle case (see above subsection), one can then show that, for all but a measure-zero set of disorder realizations in the thermodynamic limit, there exists a unique two-particle eigenstate  $|\Psi_{\alpha\beta}\rangle$  of  $U$  for each two-particle eigenstate  $|\tilde{\Psi}\rangle$  of  $\tilde{U}$  such that (up to a gauge transformation)

$$|\tilde{\Psi}\rangle = |\Psi_{\alpha\beta}\rangle + \mathcal{O}(e^{-d/\xi_t}), \quad (\text{B31})$$

and

$$\tilde{E} = E_{\alpha\beta} + \mathcal{O}\left(\frac{J d^2}{L^2}\right). \quad (\text{B32})$$

*Separated LIOMs* — Next, we consider the case where the two excited LIOMs  $\tilde{n}_1$  and  $\tilde{n}_2$  are separated by a distance  $\Delta r$  larger than  $d$ . In this case, the LIOM structure of the Floquet operator  $\tilde{U}$  (Eq. (1) in the main text) implies that, up to an exponentially small correction in the distance  $\Delta r/\xi_l$ ,  $|\tilde{\Psi}\rangle$  may be written as a direct product of two single-particle eigenstates  $|\tilde{\Psi}_\alpha\rangle$  and  $|\tilde{\Psi}_\beta\rangle$ . Here  $\alpha$  and  $\beta$  refer to the labeling of the single-particle eigenstates of  $\tilde{U}$  that was established in the previous subsection. Letting  $S_\alpha$  and  $S_\beta$  denote the two well-separated regions of linear dimension  $d$  where the states  $|\tilde{\Psi}_\alpha\rangle$  and  $|\tilde{\Psi}_\beta\rangle$  respectively have their support (up to a correction exponentially small in  $d/\xi_l$ ), we have<sup>62</sup>:

$$|\tilde{\Psi}\rangle = |\tilde{\Psi}_\alpha\rangle_{S_\alpha} \otimes |\tilde{\Psi}_\beta\rangle_{S_\beta} \otimes |0\rangle + \mathcal{O}(e^{-\Delta r/\xi_l}). \quad (\text{B33})$$

Here  $|\Psi\rangle_S$  denotes the restriction of the state  $|\Psi\rangle$  to the Fock space of the region  $S$  (defined from the projection of  $|\Psi\rangle$  into the subspace with no particles outside region  $S$ ). The state  $|0\rangle$  refers to the vacuum in the complementary region to  $S_\alpha$  and  $S_\beta$ . Since the two particles in the state  $|\tilde{\Psi}\rangle$  are separated by a distance much larger than  $d$ , the regions  $S_\alpha$  and  $S_\beta$  do not overlap.

We recall that Eq. (B16) was already proven to hold for the single-particle case. Thus  $|\tilde{\Psi}_\alpha\rangle$  is approximately identical to a single-particle eigenstate  $|\Psi_\alpha\rangle$  of the zero-flux system's Floquet operator  $U$  (for all but a measure zero set of disorder realizations). Specifically, up to a gauge transformation,  $|\tilde{\Psi}_\alpha\rangle = |\Psi_\alpha\rangle + \mathcal{O}(e^{-d/\xi_l})$ . The eigenstate  $|\Psi_\alpha\rangle$  moreover has its full support in the same region  $S_\alpha$  as  $|\tilde{\Psi}_\alpha\rangle$ , up to a correction exponentially small in  $d/\xi_l$ . Letting  $V_\alpha$  be the unitary operator that generates the transformation to the gauge in which Eq. (B16) holds for  $|\tilde{\Psi}_\alpha\rangle$ , we have

$$|\tilde{\Psi}_\alpha\rangle_{S_\alpha} = V_\alpha |\Psi_\alpha\rangle_{S_\alpha} + \mathcal{O}(e^{-d/\xi_l}). \quad (\text{B34})$$

Using the relation (B34) for the states  $|\tilde{\Psi}_\alpha\rangle_{S_\alpha}$  and  $|\tilde{\Psi}_\beta\rangle_{S_\beta}$  in Eq. (B33), and that  $\Delta r > d$ , we obtain

$$|\tilde{\Psi}\rangle = V_\alpha V_\beta |\Psi_\alpha\rangle_{S_\alpha} \otimes |\Psi_\beta\rangle_{S_\beta} \otimes |0\rangle + \mathcal{O}(e^{-d/\xi_l}). \quad (\text{B35})$$

We now note that the product of the two gauge transformations  $V_\alpha$  and  $V_\beta$  is itself a gauge transformation. We further note that, due to the LIOM structure of the Floquet operator  $U$  (Eq. (1) in the main text), the direct product  $|\Psi_\alpha\rangle_{S_\alpha} \otimes |\Psi_\beta\rangle_{S_\beta} \otimes |0\rangle$  is identical to the Floquet eigenstate  $|\Psi_{\alpha\beta}\rangle$  of the zero-flux system, up to a correction of order  $e^{-\Delta r/\xi_l}$ . We thus conclude that, up to a gauge transformation:

$$|\tilde{\Psi}\rangle = |\Psi_{\alpha\beta}\rangle + \mathcal{O}(e^{-d/\xi_l}). \quad (\text{B36})$$

The two cases we considered above show that, in the thermodynamic limit, and for all but a measure zero set of disorder realizations, *each* two-particle eigenstate  $|\tilde{\Psi}\rangle$  of  $\tilde{U}$  is identical to a unique eigenstate of  $U$ , up to a gauge transformation, and a correction of order  $\mathcal{O}(e^{-d/s})$ . Here

$A_S$  denotes the area of the region in which the state  $|\tilde{\Psi}\rangle$  has its support (up to an exponentially small correction). We may thus label the two-particle eigenstates of  $\tilde{U}$  such that Eqs. (B17) and (B16) hold with  $k = 2$ , and for each choice of the LIOM indices  $\alpha_1$  and  $\alpha_2$ .

### c. $k$ -particle-eigenstates

For the general case of a  $k$ -particle eigenstate  $|\tilde{\Psi}\rangle$  of  $\tilde{U}$ , we can apply the same structure of arguments as for the two-particle case: due to the LIOM structure of the one-flux Floquet operator  $\tilde{U}$ , each  $k$ -particle state is constructed by “exciting”  $k$  LIOMs  $\tilde{n}_1 \dots \tilde{n}_k$ . We split our line of arguments into two cases, depending on whether or not the LIOMs  $\tilde{n}_1 \dots \tilde{n}_k$  can be divided into clusters separated from each other by distances greater than  $d$ .

In the case where the excited LIOMs *can* be divided into clusters in this way,  $|\tilde{\Psi}\rangle$  can be written as a direct product of eigenstates of  $\tilde{U}$  with fewer than  $k$  particles, up to a correction of order  $e^{-d/\xi_l}$ . Following the same line of arguments as for the analogous two-particle case, the relationships (B16) and (B17) can then be demonstrated to hold for this class of eigenstates using the fact that Eq. (B16) and (B17) hold for eigenstates with less than  $k$  particles.

In the case where all LIOMs are located in the same cluster, we note that  $|\tilde{\Psi}\rangle$  only significantly overlaps with eigenstates  $\{|\Psi_{\alpha_1 \dots \alpha_k}\rangle\}$  where the centers of all the LIOMs  $\hat{n}_{\alpha_1} \dots \hat{n}_{\alpha_k}$  are located in the region  $S$ , consisting of all sites with a distance  $d$  from any of the excited LIOM's  $\tilde{n}_1 \dots \tilde{n}_k$ . There only exist a finite number of eigenstates  $N_k$  with this property. Specifically,  $N_k \lesssim \binom{kd^2/a^2}{k}$  counts the number of distinct configurations of  $k$  LIOMs  $\hat{n}_{\alpha_1} \dots \hat{n}_{\alpha_k}$  whose centers are located within  $S$ . Crucially,  $N_k$  only depends on the number of particles,  $k$ , and  $d$ , and is independent of system size.

Using the same arguments as for the single-particle case, we then find that, for all but a measure zero set of disorder realizations in the thermodynamic limit, there exists a unique eigenstate  $|\Psi_{\alpha_1 \dots \alpha_k}\rangle$  of  $U$  such that (up to a gauge transformation),

$$|\tilde{\Psi}\rangle = |\Psi_{\alpha_1 \dots \alpha_k}\rangle + \mathcal{O}(e^{-d/\xi_l}), \quad (\text{B37})$$

In addition, when the LIOMs are located within a distance  $d$  from the same point,  $\tilde{E} = E_{\alpha_1 \dots \alpha_k} + \mathcal{O}\left(\frac{Jd^2}{L^2}\right)$ . Thus, Eqs. (B16) and (B17) hold for the  $k$ -particle case in the thermodynamic limit, for any finite  $k$ .

## 5. Relationship between magnetization density and quasienergy

Having established the auxiliary results in Secs. B.1-B.4, we are now ready to prove Eq. (22) in the main text,

which is the goal of this appendix. Specifically, we show that, in the thermodynamic limit,

$$a^2 \sum_p m_{\alpha_1 \dots \alpha_k}^p = \frac{\tilde{\varepsilon}_{\alpha_1 \dots \alpha_k} - \varepsilon_{\alpha_1 \dots \alpha_k}}{B_0}. \quad (\text{B38})$$

To show this, we let  $d$  be some arbitrarily large (but finite) length such that the centers of all LIOMs  $\alpha_1 \dots \alpha_k$  are located within a disk-shaped region  $S$  of linear dimension  $d$  (recall the distance between the LIOMs must be finite for  $\varepsilon_{\alpha_1 \dots \alpha_k}$  to be nonzero). We let  $\tilde{U}$  be the one-flux Floquet operator in a gauge where Eq. (B15) holds within  $S$ , and let  $|\tilde{\Psi}_{\alpha_1 \dots \alpha_k}\rangle$  be the one-flux eigenstate corresponding to  $|\Psi_{\alpha_1 \dots \alpha_k}\rangle$  in this gauge (see previous subsection). We prove the relationship (B38) by computing the overlap  $\langle \Psi_{\alpha_1 \dots \alpha_k} | U^\dagger \tilde{U} | \tilde{\Psi}_{\alpha_1 \dots \alpha_k} \rangle$ . In the following, we make use of the shorthand notation  $\alpha = \alpha_1 \dots \alpha_k$ .

Since  $|\Psi_\alpha\rangle$  and  $|\tilde{\Psi}_\alpha\rangle$  are eigenstates of  $U$  and  $\tilde{U}$ , respectively, we have

$$\langle \Psi_\alpha | U^\dagger \tilde{U} | \tilde{\Psi}_\alpha \rangle = e^{-i(\tilde{E}_\alpha - E_\alpha)T} \langle \Psi_\alpha | \tilde{\Psi}_\alpha \rangle. \quad (\text{B39})$$

At the same time, we may write [see Eq. (B12)]

$$\begin{aligned} \langle \Psi_\alpha | U^\dagger \tilde{U} | \tilde{\Psi}_\alpha \rangle &= \langle \Psi_\alpha | \tilde{\Psi}_\alpha \rangle \\ &- i \int_0^T dt \langle \Psi_\alpha | U^\dagger(t) (\tilde{H}(t) - H(t)) \tilde{U}(t) | \tilde{\Psi}_\alpha \rangle. \end{aligned} \quad (\text{B40})$$

Note that  $|\tilde{\Psi}_\alpha\rangle$  is exponentially well localized within  $S$ , and thus  $\tilde{U}(t)|\tilde{\Psi}_\alpha\rangle = U(t)|\tilde{\Psi}_\alpha\rangle + \mathcal{O}(Jtd^2/L^2)$  [c.f. Sec. B.3]. Recalling from Eq. (B37) that  $|\tilde{\Psi}_\alpha\rangle = |\Psi_\alpha\rangle + \mathcal{O}(e^{-d/\xi_l})$ , we thus find

$$\tilde{U}(t)|\tilde{\Psi}_\alpha\rangle = U(t)|\Psi_\alpha\rangle + \mathcal{O}(e^{-d/\xi_l}), \quad (\text{B41})$$

where we suppress corrections in subleading orders of  $1/L$ .

We now note that the dual vector  $\langle \Psi_\alpha | U^\dagger(t) (\tilde{H}(t) - H(t))$  has norm of order  $\mathcal{O}(JTd^2/L^2)$  [see Eq. B14]. Using this result in Eq. (B40), along with Eq. (B41), we find

$$\begin{aligned} e^{-i(\tilde{E}_\alpha - E_\alpha)T} \langle \Psi_\alpha | \tilde{\Psi}_\alpha \rangle &= \langle \Psi_\alpha | \tilde{\Psi}_\alpha \rangle + \mathcal{O}(JTd^2e^{-d/\xi_l}/L^2) \\ &- i \int_0^T dt \langle \Psi_\alpha | U^\dagger(t) (\tilde{H}(t) - H(t)) U(t) | \Psi_\alpha \rangle. \end{aligned} \quad (\text{B42})$$

We finally note that  $\langle \Psi_\alpha | \tilde{\Psi}_\alpha \rangle = 1 + \mathcal{O}(e^{-d/\xi_l})$ . Dividing through with a factor of  $\langle \Psi_\alpha | \tilde{\Psi}_\alpha \rangle$ , and again using that  $\langle \Psi_\alpha | U^\dagger(t) (\tilde{H}(t) - H(t))$  has norm of order  $JTd^2/L^2$ , we find

$$\begin{aligned} e^{-i(\tilde{E}_\alpha - E_\alpha)T} &= 1 + \mathcal{O}(JTd^2e^{-d/\xi_l}/L^2) \\ &- i \int_0^T dt \langle \Psi_\alpha | U^\dagger(t) (\tilde{H}(t) - H(t)) U(t) | \Psi_\alpha \rangle. \end{aligned} \quad (\text{B43})$$

As a next step, we write

$$\tilde{H}(t)U(t)|\Psi_\alpha\rangle = H(B_0, t)U(t)|\Psi_\alpha\rangle + \mathcal{O}(e^{-L/\xi_l}), \quad (\text{B44})$$

where  $H(B, t)$  is the Hamiltonian of the system in the case where a uniform magnetic field  $B$  is applied throughout the torus, except for a compensating magnetic flux  $(L^2 - a^2)B$  which is applied through a plaquette  $q$ , located a distance  $\sim L$  away from  $S$  (in some properly chosen gauge). This configuration of magnetic field keeps the total flux through the torus zero, thus allowing for a continuous variation of the field  $B$ . From arguments similar to the ones made in Sec. B.2.a, one can show

$$\begin{aligned} H(B_0, t)U(t)|\Psi_\alpha\rangle &= H(t)U(t)|\Psi_\alpha\rangle + B_0 \frac{\partial H(t)}{\partial B_0} U(t)|\Psi_\alpha\rangle \\ &+ \mathcal{O}(Jd^4B_0^2). \end{aligned} \quad (\text{B45})$$

Using Eqs. (B44)-(B45) in Eq. (B43), we find

$$\begin{aligned} e^{-i(\tilde{E}_\alpha - E_\alpha)T} &= 1 - iB_0 \int_0^T dt \langle \Psi_\alpha | U^\dagger(t) \frac{\partial H(t)}{\partial B} U(t) | \Psi_\alpha \rangle \\ &+ \mathcal{O}(JTA_R e^{-d/\xi_l}/L^2), \end{aligned} \quad (\text{B46})$$

where we suppressed corrections subleading in  $1/L$  (recall  $B_0 = 2\pi/L^2$ ). Since  $|\Psi_\alpha\rangle$  is a Floquet eigenstate, we identify

$$\int_0^T dt \langle \Psi_\alpha | U^\dagger(t) \frac{\partial H(t)}{\partial B} U(t) | \Psi_\alpha \rangle = T \langle \Psi_\alpha | \overline{\frac{\partial H(t)}{\partial B}} | \Psi_\alpha \rangle \quad (\text{B47})$$

where, as in the main text,  $\overline{\mathcal{O}}$  denotes the time-average of the operator  $\mathcal{O}$  in the Heisenberg picture. Thus, we obtain

$$\begin{aligned} e^{-i(\tilde{E}_\alpha - E_\alpha)T} &= 1 - iB_0 T \langle \Psi_\alpha | \overline{\frac{\partial H(t)}{\partial B}} | \Psi_\alpha \rangle \\ &+ \mathcal{O}(JTd^2e^{-d/\xi_l}/L^2). \end{aligned} \quad (\text{B48})$$

We now recall from Sec. II.A.1 in the main text that

$$\overline{\frac{\partial H(t)}{\partial B}} = - \sum_{p \neq q} a^2 \bar{m}_p + (L^2 - a^2) \bar{m}_q. \quad (\text{B49})$$

We note that the state  $|\Psi_{\alpha_1 \dots \alpha_k}\rangle$  has its full support in the region  $S$ , up to a correction of order  $e^{-d/\xi_l}$ . Moreover,  $\bar{m}_q$  only has support in the region around plaquette  $q$ , a distance  $\sim L$  away from  $S$ . Hence  $\langle \Psi_\alpha | \bar{m}_q | \Psi_\alpha \rangle = e^{-L/\xi_l}$ . Thus, we have

$$\langle \Psi_\alpha | \overline{\frac{\partial H(t)}{\partial B}} | \Psi_\alpha \rangle = - \sum_p a^2 \langle \Psi_\alpha | \bar{m}_p | \Psi_\alpha \rangle + \mathcal{O}(e^{-L/\xi_l}). \quad (\text{B50})$$

Using this result in Eq. (B48), we find

$$\begin{aligned} e^{-i(\tilde{E}_\alpha - E_\alpha)T} &= 1 + iB_0 T \sum_p a^2 \langle \Psi_\alpha | \bar{m}_p | \Psi_\alpha \rangle \\ &+ \mathcal{O}(JTA_S e^{-d/\xi_l}/L^2). \end{aligned} \quad (\text{B51})$$

Expanding the exponential in orders of  $E_\alpha - \tilde{E}_\alpha$ , and recalling  $E_\alpha - \tilde{E}_\alpha \sim \mathcal{O}(Jd^2/L^2)$ , we conclude

$$\tilde{E}_\alpha - E_\alpha = -B_0 \sum_p a^2 \langle \Psi_\alpha | \bar{m}_p | \Psi_\alpha \rangle + \mathcal{O}(Jd^2e^{-d/\xi_l}/L^2). \quad (\text{B52})$$

Recall we may choose  $d$  arbitrarily large, and that the first term is of order  $L^{-2}$ . Thus, we conclude (restoring to earlier notation)

$$\tilde{E}_{\alpha_1 \dots \alpha_k} - E_{\alpha_1 \dots \alpha_k} = -B_0 \sum_p a^2 \langle \Psi_{\alpha_1 \dots \alpha_k} | \tilde{m}_p | \Psi_{\alpha_1 \dots \alpha_k} \rangle, \quad (\text{B53})$$

up to a relative correction that vanishes in the thermodynamic limit.

As a final step, note that [see Eq. (2) for definition of the sums]

$$E_{\alpha_1 \dots \alpha_k} = \sum_i' \varepsilon_{\alpha_n} + \sum_{i,j}' \varepsilon_{\alpha_i \alpha_j} + \dots \quad (\text{B54})$$

and

$$\langle \Psi_{\alpha_1 \dots \alpha_k} | \tilde{m}_p | \Psi_{\alpha_1 \dots \alpha_k} \rangle = \sum_i' m_{\alpha_n}^p + \sum_{i,j}' m_{\alpha_i \alpha_j}^p + \dots \quad (\text{B55})$$

Using Eq. (B53) along with the two above expansions, we can use an inductive argument akin to the one made below Eq. (13) in the main text to show that

$$\tilde{\varepsilon}_{\alpha_1 \dots \alpha_k} - \varepsilon_{\alpha_1 \dots \alpha_k} = -B_0 a^2 \sum_{\alpha_1 \dots \alpha_k} m_{\alpha_1 \dots \alpha_k}^p. \quad (\text{B56})$$

Thus, Eq. (B38) holds, which was what we wanted to prove.

### Appendix C: Analysis of model in Sec. III.A

In this appendix, we provide technical details in the analysis of the model introduced in Sec. III.A. Specifically, we will demonstrate that the invariant  $\mu_2$  takes value  $-2$  for the model. In order to do this, we identify the Floquet eigenstates of the model in the one- and two particle subspace, and subsequently use these results to infer the values of the invariants  $\mu_1$  and  $\mu_2$ .

#### 1. Classification of Floquet eigenstates

Here we identify the one- and two-particle Floquet eigenstates of the model in Sec. III.A.

*One-particle Floquet eigenstates* — In the single-particle subspace, we may set  $\hat{\Gamma}_{\mathbf{r}} = 1$  in Eq. (29), since  $\rho_{\mathbf{r},\uparrow} \rho_{\mathbf{r},\downarrow}$  gives zero when acting on any single-particle state. In this case, the Hamiltonian in Sec. III.A is identical to that of the clean-limit AFAI model studied in Refs. 9, 29, and 30, with a spinful (rather than spinless) fermion. In this case, a particle initially located on a particular site encircles a plaquette in the clockwise direction during the driving period. The Floquet operator of the system in this subspace is given by the identity, and the Floquet eigenstates of the system can be taken to be the states  $\{|\psi_{\mathbf{r},s}\rangle\}$ , where  $|\psi_{\mathbf{r},s}\rangle \equiv \hat{c}_{\mathbf{r},s}^\dagger |0\rangle$ .

*Two-particle subspace* — Next, we consider the dynamics of the system in the two-particle subspace. In this subspace, as we will show, there are three classes of initial states that result in qualitatively different time evolutions.

The first type of states is the states where the two particles are initially located on the same site  $\mathbf{r}$ . We refer to this state as  $|\psi_{\mathbf{r}}^1\rangle$ . For this class of initial states, the two particles remain confined on the same site  $\mathbf{r}$  during the full driving period, since hopping to and from the site is turned off by the operator  $\hat{\Gamma}_{\mathbf{r}}$ . Thus, letting  $U(t)$  denote the time-evolution operator of the system,  $U(t)|\psi_{\mathbf{r}}^1\rangle = |\psi_{\mathbf{r}}^1\rangle$  for all  $t$ . We refer to this class of states as class 1.

For the second type of states, the first particle is located on site  $\mathbf{r}$  in sublattice  $A$ , and the second particle is located on one of the four sites  $\mathbf{r} + \Delta\mathbf{r}_1, \dots, \mathbf{r} + \Delta\mathbf{r}_4$  on sublattice  $B$  — the two particles' spins  $s_1$  and  $s_2$  can be in any of the four possible configurations. Here  $\Delta\mathbf{r}_1 = (a, 0)$ ,  $\Delta\mathbf{r}_2 = (2a, -a)$ ,  $\Delta\mathbf{r}_3 = (a, -2a)$ , and  $\Delta\mathbf{r}_4 = (0, -a)$ . We refer to the state where the second particle is located on site  $\mathbf{r} + \Delta\mathbf{r}_n$  as  $|\psi_{\mathbf{r},n;s_1,s_2}^2\rangle$ , where  $s_1$  and  $s_2$  denote the spins of the first and second particle, respectively. During the time-evolution of  $|\psi_{\mathbf{r},n;s_1,s_2}^2\rangle$ , the two particles in the system are always located on distinct sites. However, during segment  $n$ , the two particles are located at two adjacent site connected by an active bond. Thus, the two particles do not tunnel in segment  $n$  (they still tunnel in all three remaining segments). From this fact, one can verify that the two fermions have switched places after one driving period, and hence  $U(T)|\psi_{\mathbf{r},n;s_1,s_2}^2\rangle = |\psi_{\mathbf{r},n;s_2,s_1}^2\rangle$ . Note that the phase factor of the state is 1, since each particle acquires a phase  $-i$  during each “hop”. Each particle hops 3 times, and hence, the total phase acquired is given by  $i^6 = -1$ . However, the two fermions have furthermore switched places, which means that the state acquires another factor of  $-1$ . After two driving periods, each particle has returned to its original location, after having encircled two plaquettes.

The Floquet eigenstates of the second type fall into two classes; one with quasienergy  $\pi$ , and one with quasienergy 0. The  $\pi$ -quasienergy states are the “singlet states”  $|\psi_{\mathbf{r},n}^{2S}\rangle \equiv \frac{1}{\sqrt{2}}(|\psi_{\mathbf{r},n;\uparrow\downarrow}^2\rangle - |\psi_{\mathbf{r},n;\downarrow\uparrow}^2\rangle)$ , which we refer to class 2S. The 0-quasienergy states are the remaining three “triplet combinations”  $\{|\psi_{\mathbf{r},n;i}^{2T}\rangle\}$  of the states  $\{|\psi_{\mathbf{r},n;s_1,s_2}^2\rangle, s_i = -1, 1\}$ . We refer to this class of states as class 2T.

Case 3 covers all remaining states, which are not covered by classes 1 and 2. We refer to these states as  $|\psi_{\mathbf{r}_1,s_1;\mathbf{r}_2,s_2}^3\rangle$ , such that  $|\psi_{\mathbf{r}_1,s_1;\mathbf{r}_2,s_2}^3\rangle \equiv \hat{c}_{\mathbf{r}_1,s_1}^\dagger \hat{c}_{\mathbf{r}_2,s_2}^\dagger |0\rangle$ . For this class of initial particle configurations, the particles hop in each of the four segments, and each particle encircles one plaquette in the lattice in clockwise direction. After one driving period, both particles have returned to their initial locations, and one can verify that  $U(T)|\psi_{\mathbf{r}_1,s_1;\mathbf{r}_2,s_2}^3\rangle = |\psi_{\mathbf{r}_1,s_1;\mathbf{r}_2,s_2}^3\rangle$ . We refer to this class of states as class 3.

## 2. Calculation of $\mu_2$

Having identified the one- and two-particle Floquet eigenstates of the model, we now characterize the topology of the system. The analysis in the main text concluded that  $\mu_1 = 2$ . The goal of this subsection is to use this result, along with the classification of two-particle Floquet eigenstates above to show that  $\mu_2 = -2$ . Specifically, we compute the invariant  $\mu_2$  from the response of the two-particle states' quasienergies to the insertion of a local magnetic field  $B$ .

The above subsection identified 4 classes of two-particle Floquet eigenstates in the model (1,  $2S$ ,  $2T$  and 3). The Floquet eigenstates of type 1 do not result in any current in the system, and their quasienergies are unaffected by the magnetic field. For the Floquet eigenstates of type  $2S$  and  $2T$ , one can verify that each of the two particles encircle two plaquettes after two driving periods, in clockwise direction (at this point, the final state is identical to the initial state). Hence these Floquet eigenstates pick up an additional phase  $-2Ba^2$  after a single driving period. The quasienergies of the type  $2S$  Floquet eigenstate in the presence of the field  $B$  is thus given by  $\pi/T - 2Ba^2/T$ , while the quasienergy of the type  $2T$  Floquet eigenstate is given by  $-2Ba^2/T$ . For the type-3 Floquet eigenstates, each particle encircles a plaquette clockwise during the driving period, and

hence picks up a phase of  $-2Ba^2$ . We thus conclude that  $\frac{\partial E}{\partial B} = -2a^2/T$ , and hence  $\langle \bar{M} \rangle = 2a^2/T$  for the Floquet eigenstates in classes  $2S, 2T, 3$ . For Floquet eigenstates of type 1,  $\frac{\partial E}{\partial B} = 0$ , and hence  $\langle \bar{M} \rangle = 0$ .

We note that there are  $D/2$  distinct two-particle Floquet eigenstates in class 1 (where  $D = 2L^2/a^2$  is the number of distinct single-particle states); hence there are  $\binom{D}{2} - D/2$  distinct states of type  $2S, 2T$ , and 3. Since  $\langle \bar{M} \rangle = 2a^2/T$  for Floquet eigenstates of type  $2S, 2T$ , and 3, while  $\langle \bar{M} \rangle = 0$  for Floquet eigenstates of type 1, we conclude

$$\text{Tr}_2 \bar{M} = \frac{2a^2}{T} \left[ \binom{D}{2} - D/2 \right]. \quad (\text{C1})$$

Using Eq. (30), we find that

$$\mu_2 = \mu_1 \binom{D-1}{1} - \frac{\text{Tr}_2 \bar{M}}{L^2}. \quad (\text{C2})$$

Above, we concluded that  $\mu_1 = 2$ . Using  $D = 2L^2/a^2$ , along with Eq. (C1), one can verify

$$\mu_2 = -2. \quad (\text{C3})$$

This was what we set out to show.